universität wien

MASTERARBEIT

Titel der Masterarbeit

Quantum Phase Transition in coupled 1-d Bose Einstein condensates

Verfasser

Stefan Beck BSc.

angestrebter akademischer Grad

Master of Science (MSc)

Wien, 2014

Studienkennzahl lt. Studienblatt:	066876
Studienrichtung lt. Studienblatt:	Masterstudium Physik
Betreuer:	Univ.-Prof. Dr. Norbert J. Mauser

Zusammenfassung

Die Hauptziele dieser Arbeit waren die numerische Untersuchung der Effekte eines künstlichen Eichfeldes auf zwei durch den Tunneleffekt verbundene eindimensionale Bose–Einstein–Quasikondensate und die Suche nach einem Quantenphasenübergang. Hierzu mussten zwei gekoppelte stationäre *Gross-Pitaevskii* Gleichungen gelöst werden. Mit dem Absolutquadrat der erhaltenen Lösungen sind die Dichteverteilungen der Quasikondensate im Grundzustand darstellbar. Es wurde die häufig benutzte *Imaginäre Zeitpropagation* in Kombination mit der *Split–Operatoren–Methode* in erster Ordnung verwendet um die Grundzustände zu berechnen. In einem ersten Teilschritt wurden zuerst die Grundzustände der ungekoppelten und ungestörten Quasikondensate ermittelt. Die Ergebnisse entsprechen der erwarteten Form, denn erst durch den Einfluss des künstlichen Eichfeldes entsteht eine spezielle Quantenwirbelstruktur, die zu periodischen Oszillationen in den Dichteverteilungen der nun tunnelgekoppelten eindimensionalen Kondensate führt. Mit erhöhter Tunnelwahrscheinlichkeit der Partikel zwischen den Kondensaten sieht man in den numerischen Simulationen einen Quantenphasenübergang zu energetisch bevorzugten Dichteverteilungen. Nach dem Phasenübergang zeigen diese Grundzustandsprofile, ähnlich denen der ungestörten und ungekoppelten Grundzuständen, keinerlei Oszillationen.

Abstract

The main goals of this study were the numerical investigation of the effects of an artificial gauge field applied on two tunnel-coupled one–dimensional Bose–Einstein quasi–condensates and to search for a quantum phase transition in a certain parameter range. In order to achieve this goal two coupled stationary *Gross–Pitaevskii equations* had to be solved. The squared solutions represent the density profiles of the condensates in their ground states. The widely used method called *imaginary time propagation* combined with the *time-splitting spectral* method was applied to compute these ground states. In a first partial result of this study it was shown, that both of the uncoupled and undisturbed quasi–condensates possess uniform density distributions. Through the applied artificial gauge field a special structure of quantum vortices emerged, which led to periodical oscillations in the ground–state density profiles of the now tunnel–coupled one–dimensional Bose–Einstein condensates. For a higher tunnelling probability of particles between the BECs, the expected quantum phase transition to an energetically more favourable density distribution occurs regarding to the numerical computations. These profiles after the quantum transition show no oscillations similar to the unaffected ground state profiles.

Acknowledgements

First of all I would like to thank my advisors, Prof. Norbert J. Mauser and Dr. Igor E. Mazets for the opportunity to do this master thesis on such an interesting challenging problem at the interface of quantum physics and applied mathematics.

I am grateful to Dr. Mazets for his tremendous support, for sharing his deep knowledge of physics with me - and for his patience.
I am grateful to Prof. Mauser for taking over the supervision of the modeling and numerical work and the thesis as a whole.

I am especially grateful to Dr. Hans Peter Stimming from Prof. Mauser's group at the Wolfgang Pauli Institute for his crucial help in the numerical methods and simulations as well as his corrections in the writing up of the numerical part of the thesis.

All the conversations with the members of the Institute of Atomic and Subatomic Physics, especially from the Atomchip Group lead by Prof. Jörg Schmiedmayer, enabled me to accomplish this study.

Mag. Karoline Mühlbacher BSc. my safe haven in a rough sea

Danken möchte ich vorallem auch meiner Mutter Klaudia Beck für die jahrelange Unterstützung während meines Studiums.

Mag. Michael Rammerstorfer – a very supportive lifelong dear friend

Mag. Mag. Lukas Mairhofer – kluk

Mag. Bakk. Birgit Trappl – the latex wizardess

Contents

1 Introduction **1**

1.1 Bose Einstein Condensate 1
1.2 Second Quantisation 3
1.3 Bogoliubov approximation 5
1.4 Artifical gauge field 8
1.5 Superfluidity 15
1.6 Quantized Vortices 16
1.7 Dimensionality and quasi condensates 18

2 How to trap and cool atoms **21**

2.1 Laser cooling 21
2.2 Magneto Optical Trap 25
2.3 Evaporative cooling 26

3 Numerical models and methods **29**

3.1 Gross–Pitaevskii equation: Standard model for BEC 29

4 Two coupled 1–d Bose Einstein condensates **34**

4.1 Imaginary time propagation 35
4.2 Dimensionless GPE 36

5 Computations **39**

5.1 Ground state 39
5.2 Applying the artificial gauge field 40
5.3 Results 41
5.4 Interpretation 42

6 Outlook **47**

A Mathematica code **48**

A.1 Ground state 48
A.2 Coupled BECs 49

References **51**

Curriculum Vitae **55**

1 Introduction

1.1 Bose Einstein Condensate

In 1924 Satyendra Nath Bose wrote a short paper [8], which Einstein himself translated for publication in Bose's name in *Zeitschrift für Physik*. In his work Bose studied the statistical property of massless, non−interacting bosonic particles nowadays known as *photons*. They are described by the Bose−Einstein statistics. The number expectation value of non-interacting bosons in thermodynamic equilibrium in the i^{th} energy state with $\epsilon_i > \mu$ is given by

$$n_i(\epsilon_i) = \frac{g_i}{e^{(\epsilon_i - \mu)/k_B T} - 1} \tag{1}$$

where μ is the chemical potential, ϵ_i is the energy of the i^{th} state, g_i is the degeneracy of the i^{th} state, k_B is the Boltzmann constant and T is the absolute temperature. This becomes approximately the Boltzmann-distribution at high temperatures, when quantum effects are negligible. Einstein recognized the significance of Bose's work and generalized it to a model of an ideal gas of massive bosons, drawing the map to the basic idea of Bose−Einstein condensate (BEC).
At sufficiently low temperatures a dilute Bose gas undergoes a quantum phase transition into another state. According to the Bose−Einstein statistics an infinite number of particles can occupy the same energy state, therefore a large fraction of particles will occupy the lowest energy ground state. Thus quantum effects appear on a macroscopic scale.

The center particle density at Bose-Einstein condensed atomic clouds is between $10^{13} - 10^{15} cm^{-3}$, in comparison to the density of air at room temperature and atmospheric pressure is around $10^{19} cm^{-3}$. In solids the density is about $10^{22} cm^{-3}$. At the low densities of a BEC the temperature in the system must be in the order of 10^{-5}K or less to see quantum phenomena. One of the major advantages of studying quantum phenomena in cold gas clouds is that almost all the atoms occupy the same quantum state, and therefore can be described within the mean-field theory. This approach is comparable with the Hartree-Fock theory for atoms, which describes liquids in the absence of strong interactions between the atoms, like in liquid ^{4}He. A further advantage of studying systems at these low densities is that the "microscopic" length scales are large, so that they can be studied by optical means.[24, p. 2.]

The onset of Bose-Einstein condensation in an atomic cloud of bosonic particles is related to a transition temperature T_C. A connection between the particle density and the transition temperature can be established by comparing the inter–particle distance

with the thermal de Broglie wavelength, which is defined as follows:

$$\lambda_T = \left(\frac{2\pi\hbar^2}{mk_BT} \right)^{1/2} \tag{2}$$

where $\hbar$ is the reduced Planck constant, defined via the Planck constant by $h = 2\pi\hbar$. At high temperatures a gas behaves classically and its de Broglie wavelength is small. In early experiments for alkali atoms this is true for densities of the order of $10^{13} cm^{-3}$. Nowadays experimental setups work with densities in the range of $10^{14} - 10^{15} cm^{-3}$ with transition temperatures ranging from 100 nK to the order of μK.[24, s. 5.] At high temperatures the chemical potential is significantly smaller than the lowest single particle state energy, therefore any state's mean occupation number is less than unity, and therefore $exp\left[(\mu - \epsilon_{min})\right] \ll 1$. Trapped gases are not uniform because they are confined by a potential, which is harmonic in the most cases.

The transition temperature T_C is the temperature at which the macroscopic occupation of lowest energy state begins. In a 3-dimensional harmonic oscillator potential, the transition temperature is given by[9]

$$k_BT_C = \frac{\hbar\bar{\omega}N^{1/3}}{\left[\zeta\left(3\right)\right]^{1/3}} \approx 0.94\hbar\bar{\omega}N^{1/3} \tag{3}$$

where $\bar{\omega} = \left(\omega_1\omega_2\omega_3\right)^{1/3}$ is the geometrical mean of the oscillator frequencies in all the three spatial dimensions and $\zeta\left(3\right)$ the Riemann zeta function, which is defined by $\zeta\left(\alpha\right) = \sum_{n=1}^{\infty} n^{-\alpha}$ and N is the number of particles

$$T_C \approx 4.5 \left(\frac{\bar{\nu}}{100Hz} \right) N^{1/3} nK \tag{4}$$

where $\bar{\nu} = \bar{\omega}/2\pi$ [24, s. 21f.]
For $T < T_C$ the number of thermal excited particles is given by

$$N_e = N \left(\frac{T}{T_C} \right)^d \tag{5}$$

with the chemical potential $\mu = 0$ and where d is the number of dimensions. Following from that the number of particles N_0 in the condensate is

$$N_0\left(T\right) = N - N_e\left(T\right) = N \left[1 - \left(\frac{T}{T_C} \right)^d \right] \tag{6}$$

The occurrence of a sudden transition for $T/T_C \sim 1$ is obvious. The same result one

gets by computing

$$N - N_0 = \int_0^\infty \frac{\rho(\epsilon)\, d\epsilon}{exp(\epsilon/k_B T) - 1} \tag{7}$$

where $\rho(\epsilon)$ is the density of states depending on the energy ϵ. This density, in case of plane waves of energy $\epsilon = p^2/(2m)$ being eigenstates of the Hamiltonian, is given by

$$\rho(\epsilon) = \frac{1}{(2\pi)^2} L^3 \left(\frac{2m}{\hbar^2}\right)^{3/2} \sqrt{\epsilon}, \tag{8}$$

where L^3 is the volume, the number of dimensions is d equals 3. Another point of interest is the density of thermal particles $n_T(\mathbf{r})$ calculated under a semiclassical approximation. The total density $n(\mathbf{r})$ is given by the sum of the thermal particle density $n_T(\mathbf{r})$ and the condensed particle density $n_0(\mathbf{r}) = N_0|\phi_0(\mathbf{r})|^2$. Thus $n(\mathbf{r})$=$n_T(\mathbf{r}) + n_0(\mathbf{r})$. For temperatures below the critical value and taking the thermodynamical limit, number of particles $N \to \infty$, size of the volume $L^3 \to \infty$ and the density $N/V = const$, the thermal density is given by

$$n_T(\mathbf{r}) = \int d\mathbf{p} \frac{1}{(2\pi\hbar)^3} \frac{1}{exp(\beta\ \epsilon(\mathbf{p}, \mathbf{r})) - 1} \tag{9}$$

the integral over the momentum space, where $\epsilon(\mathbf{p}, \mathbf{r}) = p^2/2m + v_{ext}(\mathbf{r})$ is the semiclassical energy in phase space. This yields

$$n_T(\mathbf{r}) = \lambda_T^{-3} g_{3/2}\left(e^{-\beta v_{ext}(\mathbf{r})}\right), \tag{10}$$

where $\lambda_T = \left[2\pi\hbar^2/(mk_B T)\right]^{1/2}$ is the thermal wavelength. The function $g_{3/2}(\mathbf{r})$ is defined via $g_\alpha = \sum_{n=1}^\infty z^n/n^\alpha$. If one integrates $n_T(\mathbf{r})$ over the whole space one will arrive again at the number of atoms, which are removed from the condensate due to thermal effects $N - N_0 = N(T/T_C)^3$. In the same manner one can compute the thermal distribution in momentum space:[9, p. 469.]

$$n_T(\mathbf{p}) = \frac{1}{(\lambda_t m\omega_0)^3} g_{3/2} \frac{1}{exp\left[\frac{\beta p^2}{2m}\right]} \tag{11}$$

1.2 Second Quantisation

Second Quantisation was introduced by Jordan, Klein and Wigner in the year 1928. [18] It describes the quantisation of fields and therefore can be used in a wider range than quantum mechanics. Quantum mechanics suits single quantum systems best, but meets its limits if applied on a many body system. If one works with many body systems the clear choice is the second quantisation. Every potential with a local minimum can be described approximately around the equilibrium point by a harmonic potential. The

non–degenerate energy levels of the harmonic potential are $E_n = \hbar\omega\left(n + \frac{1}{2}\right)$. For N indistinguishable particles in a one dimensional harmonic trap the Hamiltonian reads as follows

$$H = \sum_{m=1}^{N}\left(-\frac{\hbar^2}{2m}\nabla_m^2 + m\omega^2 z_m^2\right) + \frac{1}{2}\sum_{m,n=1;m\neq n}^{N} V\left(z_m - z_n\right) \tag{12}$$

where $V\left(z_m - z_n\right)$ is the interaction potential.

$$V\left(z_m - z_n\right) = g\delta\left(z_m - z_n\right) \tag{13}$$

The N–body wave function $\Psi\left(z_1, z_2, ..., z_N, t\right)$ is the superposition of products of single particle stationary wave functions $\phi_{m_i}\left(z_i\right)$

$$\Psi\left(z_1, z_2, ..., z_N, t\right) = \sum_{m_1,m_2,...,m_N} F\left(m_1, m_2, ...m_N, t\right)\phi_{m_1}\left(z_1\right)\cdot\phi_{m_2}\left(z_2\right)\cdot...\cdot\phi_{m_N}\left(z_N\right) \tag{14}$$

The many body wave function is symmetric in case of bosons and antisymmetric for fermions.
This means that in the case of commutation of two particles the following relation is true for bosons,

$$\Psi\left(..., z_m, ..., z_n..., t\right) = \Psi\left(..., z_n, ..., z_m, ..., t\right) \tag{15}$$

whereas the many body wave function for fermions under the same conditions is:

$$\Psi\left(..., z_m, ..., z_n..., t\right) = -\Psi\left(..., z_n, ..., z_m, ..., t\right) \tag{16}$$

Every quantum state is uniquely defined and completely described by a set of occupation numbers n_1,n_2,...,n_N associated with the Energy levels E_1,E_2 and so on. A quantum state vector in Fock space is defined by the according $|n_1, n_2, ...n_m, ...\rangle$.
The annihilation and creation operators are defined for the energy eigenstates of the system.
The operator $\hat{a}_m^\dagger$ creates a particle in an energy eigenstate with the energy level E_m

$$\hat{a}_m^\dagger|n_1 n_2 ... n_m ...\rangle = \sqrt{n_m + 1}|n_1 n_2 ... \left(n_m + 1\right) ...\rangle \tag{17}$$

whereas the annihilation operator destroys one particle from the m^{th} energy level

$$\hat{a}_m|n_1 n_2 ... n_m ...\rangle = \sqrt{n_m}|n_1 n_2 ... \left(n_m - 1\right) ...\rangle \tag{18}$$

Both fullfill the following commutator relations

$$[\hat{a}_m, \hat{a}_m] = 0 \tag{19}$$
$$\left[\hat{a}_m^\dagger, \hat{a}_m^\dagger\right] = 0 \tag{20}$$
$$\left[\hat{a}_m, \hat{a}_m^\dagger\right] = \delta_{ij} \tag{21}$$

The field operators in the second quantisation are defined by

$$\hat{\psi}(z,t) = \sum_n a_n \phi(z) \tag{22}$$

$$\hat{\psi}^\dagger(z,t) = \sum_n a_n^\dagger \phi_n^\star(z) \tag{23}$$

Like the creation operator $\hat{a}^\dagger$, the field operator $\hat{\psi}(z,t)$ creates a particle at the spatial position z at a certain time t when applied on the vacuum state.
The following commutator relations are true for the field operators

$$\left[\hat{\psi}(z,t), \hat{\psi}(z',t)\right] = 0 \tag{24}$$
$$\left[\hat{\psi}^\dagger(z,t), \hat{\psi}^\dagger(z',t)\right] = 0 \tag{25}$$
$$\left[\hat{\psi}(z,t), \hat{\psi}^\dagger(z',t)\right] = \delta_{zz'} \tag{26}$$

The "second quantizied Hamiltonian $\hat{H}$" is obtained from the expectation values of the Hamiltonian with field operators $\hat{\psi}^\dagger(z,t)$ and $\hat{\psi}(z,t)$.
The single particle Hamilton operator is

$$\hat{H}_0 = \int dz\ \hat{\psi}^\dagger(z,t) \left[-\frac{\hbar^2}{2m}\nabla^2 + m\omega^2 z^2\right] \hat{\psi}(z,t) \tag{27}$$

The interactions between two particles is described by the following operator

$$\hat{V} = \frac{1}{2}\int\int dz\ dz'\ \hat{\psi}^\dagger(z)\,\hat{\psi}^\dagger(z')\,V(z,z')\,\hat{\psi}(z')\,\hat{\psi}(z) \tag{28}$$

Inserting the inter–particle potential in the Dirac delta form from above reduces the double to a single integral:

$$\hat{V} = \frac{1}{2}\int dz\ \hat{\psi}^\dagger(z)\,\hat{\psi}^\dagger(z')\,\hat{\psi}(z')\,\hat{\psi}(z) \tag{29}$$

1.3 Bogoliubov approximation

In the presence of BEC, the ideal Bose gas has a constant pressure against variation of volume, so that the system features infinite compressibility. This pathological feature originates from the absence of particle-particle interaction. Therefore, it is not sur-

prising that interactions between particles affect the properties of the gas in a dramatic way, even for very dilute samples. [30, chap. 4., p. 1.]

The range z_{IAF} of forces between particles in a dilute gas is far smaller than the averaged distance d between the particles

$$z_{IAF} \ll d = n^{-\frac{1}{3}} = \left(\frac{N}{V}\right)^{-\frac{1}{3}} \tag{30}$$

If the distance between two particles z is smaller than z_{IAF} then the interaction between the atoms is non-zero. $V(z)$ is a two body scattering potential depending on the interparticle distance z.

$$\tilde{V}(p) = \int V(z)\, e^{ip\cdot z/\hbar} dz \tag{31}$$

is the Fourier transform of $V(z)$, where the scattering amplitude is independent of the momentum as long as $p \ll \hbar/z_{IAF}$. The investigated ensemble is called a dilute gas, if it fulfills the the approximation that $z_{IAF} \ll d$ and therefore only two body processes have to be taken into consideration and all interactions of three and more bodies can be ignored. Its temperature must be small enough so that the thermal component of the momentum distribution is substantially smaller than $p_0 = \hbar/z_0$

$$T \ll \frac{\hbar^2}{2mk_B z_0^2} \tag{32}$$

.

The low energy scattering amplitude V_0 is defined by the s-wave scattering length a_s as follows

$$V_0 = \frac{\pi\hbar^2}{m} a_s \tag{33}$$

The Bogoliubov perturbation theory is applicable on a system if it meets the diluteness condition

$$|a_s| n^{\frac{1}{3}} \ll 1 \tag{34}$$

The second quantizied Hamiltonian with the field operators $\hat{\psi}$, the scattering potential between two particles $V(\mathbf{r}, \mathbf{r}')$ takes the following form

$$\hat{H} = \int d\mathbf{r} \left(\frac{\hbar^2}{2m} \nabla\hat{\psi}^\dagger(\mathbf{r}) \nabla\hat{\psi}(\mathbf{r})\right) + \frac{1}{2}\int\int d\mathbf{r} d\mathbf{r}' \hat{\psi}^\dagger(\mathbf{r}) \hat{\psi}^\dagger(\mathbf{r}') V(\mathbf{r}', \mathbf{r}) \hat{\psi}(\mathbf{r}) \hat{\psi}(\mathbf{r}') . \tag{35}$$

The field operators can be expanded to plane wave form, if the gas occupies a cubic volume L^3.

$$\hat{\psi}(\mathbf{r}) = \frac{1}{\sqrt{L^3}} \sum_p \hat{a}_p e^{ipr/\hbar} \tag{36}$$

where $\hat{a}_p$ is the annihilation operator acting on single particle states of a plane wave

with the momentum p. Together with the Fourier transform of the two-body scattering potential V_q the Hamiltonian in the momentum regime takes the form

$$\hat{H} = \sum_p \frac{p^2}{2m} \hat{a}_p^\dagger \hat{a}_p + \frac{1}{2L^3} \sum_{p_1,p_2,q} V_q \hat{a}_{p_1+q}^\dagger \hat{a}_{p_2-q}^\dagger \hat{a}_{p_1} \hat{a}_{p_2} \tag{37}$$

The potential in real systems always inhabits short range terms, which makes it difficult to find the correct analytical solution to the Schrödinger equation on small scales. But it is easy to see, that in the diluteness of the gas, which is dealt with, the real $V(r)$ with its difficulties for $z < z_{IAF}$ does not contribute to the macroscopic behaviour. Therefore it can be replaced by an assumed potential $V_{eff}(z)$. The only condition to this assumed potential is, that its Fourier transform $V_{q \ll \hbar/z_{IAF}}$ gives the correct value in the low momentum range. The macroscopic properties depend on $V_{q=0} = V_0$ or the s-wave scattering length, therefore the replacement will deliver the correct solutions for a complex system as long as it meets the following conditions: It has to be sufficiently cold and dilute and the lowest energy state has to be occupied by a macroscopic fraction of the particles; one can neglect quantum fluctuation of this state and replace $\hat{a}_0 \equiv \sqrt{N_0}$; furthermore the occupation number for excited states with $p \neq 0$ needs to be small so that it can be neglected in the lowest order approximation for our Hamiltonian above. The ground state energy then takes the form

$$E_0 = \frac{V_0}{2L^3} N_0^2 \cong \frac{V_0}{2L^3} N^2 \tag{38}$$

where V_0 in the Born approximation is given by

$$V_0 = \frac{4\pi\hbar^2 a_s}{m} = g \tag{39}$$

From

$$P \equiv -\frac{\partial E_0}{\partial L^3} = \frac{g}{2} n^2 \tag{40}$$

where $n = N/L^3$ is the particle density, we see that the pressure of the Bose Einstein condensate in a dilute gas is always non-zero, also for $T = 0$. The thermochemical stability requires that the compressibility

$$\frac{\partial n}{\partial P} = \frac{1}{gn} \tag{41}$$

is positive, that means $g > 0$ and the s-wave scattering length $a_s > 0$ respectively. In conclusion from the previous, one can conclude that a stable, dilute BEC can only exist in systems with repulsive interactions.

From this we also get the chemical potential

$$\mu \equiv \frac{\partial E_0}{\partial N} = gn = mc^2 \tag{42}$$

$\mu > 0$ for all temperatures, even for $T = 0$ and defines the energy needed or gained for adding or removing one particle from the Bose Einstein condensate respectively.

1.4 Artifical gauge field

Charged particles can be accelerated or retarded by electric or magnetic fields, but if uncharged atoms are the subject of interest these means are not applicable. If a neutral atom moves through a laser light field which is tuned appropriately, the trajectory of the uncharged particles matches the path of a charged particle in a magnetic field with a Lorentz-like force. In the quantum mechanical picture the orbital magnetism of an e^- can be interpreted as a consequence of the Aharonov–Bohm phase γ, which a particle gains while moving along the closed curve $\mathcal{C}$. The magnitude is independent of the particle's velocity, because the phase $\gamma = 2\pi\Phi/\Phi_0$ is of geometric origin. Φ is the flux of the magnetic field through the curve $\mathcal{C}$ and $\Phi_0 = h/e$ is the flux quantum [12, p. 1524.]. For the realization of artificial magnetism for a neutral particle, one must search for a setting which adds a geometrical phase to the particle during its movement on a full cycle on $\mathcal{C}$. Mathematically this is described by a unitary operator U, which is defined on an internal Hilbert space and is dependent only on the geometry of the path $\mathcal{C}$. The particle is transferred from the internal state $|\psi_i\rangle$ to another internal state $U|\psi_i\rangle$.

Berry phase - a simple example for a geometric phase

Considering a particle with magnetic moment μ in an inhomogeneous magnetic field $B_0(\mathbf{r})$. At the position $\mathbf{r}_0$ the particle is initially in one of the eigenstates $|m(\mathbf{r}_0)\rangle$ of the Hamiltonian

$$H = -\mu \mathbf{B}_0(\mathbf{r}) \tag{43}$$

If the particle's velocity is adequately slow, it follows adiabatically the local eigenstate $|m(\mathbf{r}_t)\rangle$. After one circumnavigation of $\mathcal{C}$ is completed, the particle returns to the internal state $|m(\mathbf{r}_0)\rangle$ gaining a geometrical phase.
The Berry phase emerges also from atom–light interactions. The eigenstates of atom–light coupling, called *dressed states*, take the former position of the magnetic states $|m(\mathbf{r})\rangle$. According to Dalibard et al. [12] the dressed states are variable on short spatial scale (typically: the wavelength λ of the light) and the artificial gauge fields are considerably intense. Implying that the geometric phase γ is large in relation to 2π of

a curve enclosing an atom cloud of realistic size.

Simple model: two level atom in a laser beam

An atom with two internal states following one of the states adiabatically can provide the desired gauge field. The basis for the two dimensional Hilbert space $\{|g\rangle, |e\rangle\}$ is represented by the ground state and the excited state of the atom. The particle is driven by space-dependent external fields that couple to the two internal states $|g\rangle$ and $|e\rangle$ of the atom. In general the Hamiltonian of the particle without specifying the origin of the external field is given by

$$H = \left(\frac{P^2}{2M} + V\right)\hat{I} + U \tag{44}$$

where M is the mass of the particle, $\hat{I}$ is the identity operator on the Hilbert space, $P = -i\hbar\nabla$ represents the quantum mechanical momentum operator and U is the coupling operator which is defined as follows:

$$U = \frac{\hbar\Omega_R}{2}\begin{pmatrix} \cos\theta & e^{-i\phi}\sin\theta \\ e^{i\phi}\sin\theta & -\cos\theta \end{pmatrix}. \tag{45}$$

The behaviour of the atom is determined by four real quantities: The potential V influences the particle independent of its internal state. The Rabi frequency Ω_R, the frequency of the oscillation of the atomic transitions in the light field, gives a measure of the strength of the coupling. The other two quantities are the mixing angle θ and the phase angle ϕ. In the case of a two level system $\Omega_R \cos\phi$ stands for the laser detuning $\delta = \omega - \omega_0$ from the atomic resonance and $\Omega_R \sin\phi$ is the magnitude of the atom–laser coupling and ϕ is the laser phase [12].

Adiabatic following

The eigenstates of the coupling matrix U are

$$|\chi_1\rangle = \begin{pmatrix} \cos(\theta/2) \\ e^{i\phi}\sin(\theta/2) \end{pmatrix} \tag{46}$$

$$|\chi_2\rangle = \begin{pmatrix} -e^{-i\phi}\sin(\theta/2) \\ \cos(\theta/2) \end{pmatrix} \tag{47}$$

with the associated eigenvalues $\hbar\Omega/2$ and $-\hbar\Omega/2$.
The name *dressed states* means the states do not solely contain the isolated atom or particle but also the perturbation, the interaction and the coupling between the atom and the light field. The eigenstates of the matrix form an orthonormal basis $\{|\chi_j\rangle\}$ of

the internal Hilbert space. Therefore the statement that $i\langle\chi_j|\nabla\chi_j\rangle \in \mathbb{R}$ is true and the relation $\langle\nabla\chi_2|\chi_1\rangle = -\langle\chi_2|\nabla\chi_1\rangle$ holds, where $|\nabla\chi_j\rangle \equiv \nabla\left(|\chi_j\rangle\right)$.
The full state of the particle can be written as a superposition of the dressed states

$$|\Psi\left(\mathbf{r},t\right)\rangle = \sum_{j=1,2} \psi_j\left(\mathbf{r},t\right)|\chi_j\left(\mathbf{r}\right)\rangle \tag{48}$$

At an initial time a particle is created in one of the two dressed states, in this case $|\chi_1\rangle$ is chosen. If the velocity distribution contains only sufficiently small components, the internal state will always be proportional to the original dressed for all time.[12] This can be seen as an analogon to the Born-Oppenheimer approximation: The position and the internal degrees of freedom play the role of the nuclear coordinates and the electron dynamics, respectively.

Of interest are also the effects if the quantum mechanical momentum operator $\mathbf{P}$ acts on the full state vector $|\Psi\rangle$. With $\nabla\left[\psi_j|\chi_j\rangle\right] = \left[\nabla\psi_j\right]|\chi_j\rangle + \psi_j|\nabla\chi_j\rangle$ and the completeness relation, one gets

$$\mathbf{P}|\Psi\rangle = \sum_{j,l=1}^{2}\left[\left(\delta_{j,l}\mathbf{P} - \mathbf{A}_{jl}\right)\psi_l\right]|\chi_j\rangle \tag{49}$$

with $\mathbf{A}_{jl}\left(\mathbf{r}\right) = i\hbar\langle\chi_j|\nabla\chi_l\rangle$. To compute the equation of motion for ψ_1 one must assume $\psi_2 = 0\forall t$, which means that ψ_2 is negligible for all times. Then the Schrödinger equation $i\hbar|\dot{\Psi}\rangle = H|\Psi\rangle$ is projected on the internal dressed state $|\chi_1\rangle$, where H is the Hamiltonian in (44). This leads to an equation for the probability amplitude ψ_1 to find the particle in the first dressed state [12, p. 1525.], which is written as follows

$$i\hbar\frac{\partial\psi_1}{\partial t} = \left[\frac{\left(\mathbf{P}-\mathbf{A}\right)^2}{2M} + V + \frac{\hbar\Omega}{2} + W\right]\psi_1 \tag{50}$$

Two new geometric potentials $\mathbf{A}$ and W arise in the adiabatic elimination of $|\chi_2\rangle$, whereas V and $\hbar\Omega_R$ already appeared in the original Hamiltonian in (44). Reason for this is that the dressed states depend on the spatial position $\mathbf{r}$.
$\mathbf{A}$ is the vector potential

$$\mathbf{A}\left(\mathbf{r}\right) = i\hbar\langle\chi_1|\nabla\chi_1\rangle = \frac{\hbar}{2}\left(\cos\theta - 1\right)\nabla\phi \tag{51}$$

The effective magnetic field related to the vector field $\mathbf{A}$ is

$$\mathbf{B}\left(\mathbf{r}\right) = \nabla\times\mathbf{A} = \frac{\hbar}{2}\nabla\left(\cos\theta\right)\times\nabla\phi \tag{52}$$

If this artificial magnetic field does not vanish, the vector potential **A** cannot be eliminated by gauge transformations from the differential equation for the probability amplitude ψ_1 in (50). The particle's trajectory mimics the motion of a particle with orbital magnetism by an effective charge it obtained by adiabatically following the dressed state. The condition for $\mathbf{B} \neq 0$ is that the mixing angle θ and phase angle ϕ vary in space with noncollinear gradients. The second geometrical potential in (50) is the positive scalar term [12, p. 1526.]

$$W(\mathbf{r}) = \frac{\hbar^2}{2M}|\langle\chi_2|\nabla\chi_1\rangle|^2 = \frac{\hbar^2}{8M}\left[(\nabla\theta)^2 + \sin^2\theta\,(\nabla\phi)^2\right]. \tag{53}$$

The reason for the vector fields **A**, **B** and scalar field W being called *geometric* is their dependency on the spatial variation of the two angles θ and ϕ, i.e. the geometry of the coupling between $|g\rangle$ and $|e\rangle$ and not on the strength Ω_R of the coupling.
Remark: If one would have computed the adiabatic following of the dressed state χ_2 instead of χ_1, one would have seen an equation of motion composed of the same scalar potential W but with an opposite vector field **-A** [12, p. 1526.].

The question arises how the mechanism and schemes discussed above can be used in real life experiments to create artificial orbital magnetism in dilute gases of cold atoms respectively BECs. To target atoms with a single laser beam, whose frequency ω_L is marginally detuned from the resonant atomic transition frequency ω_A between two internal states $|g\rangle$, which is called ground state, and $|e\rangle$, called electronically excited state poses a simple approach. We assume that the depletion of the excited state $|e\rangle$ through emission or, more precisely, the rate of spontaneous emission of photons from the excited state $|e\rangle$ is negligible on the relevant time scale.
For example in real experiments with alkaline earth atoms (^{20}Ca,^{30}Sr) and the lanthanide series ^{70}Yb it was shown that the radiative lifetime of the excited state $|e\rangle$ is of the order of seconds or even tens of seconds. This is much longer than the average experiment with dilute cold atoms lasts.

Physical interpretation of emerging geometric potentials

In two level systems as discussed before the scalar potential W can be understood as the kinetic energy associated with the fast microscopic motion of the particle first explained for a classical continuous internal degree of freedom by Aharonov and Stern (1992). A particle in the internal state $|\chi_1\rangle$ with a center of mass state is represented by a wave package localized around position **r** with side tails which are small compared to the variation scale of θ and ϕ. [12, p. 1528.] Dalibard et al. introduced the force operator $\mathbf{F} = -\nabla U$ and stressed that the eigenstates $|\chi_j\rangle$ of the coupling matrix U do not coincide with the eigenstates of the operator **F**. The force shows quantum

fluctuations with $\langle \mathbf{F} \rangle^2 \neq \langle \mathbf{F}^2 \rangle$ and a nonzero uncertainty, which means $\Delta \mathbf{F} \neq 0$. In the Heisenberg picture the quantum states are independent of time such that $|\psi\rangle = const$ and the operators are time dependent, i.e. $\hat{A} = \hat{A}(t)$. The dynamics of the system are described by the Heisenberg equation, which is defined as

$$\frac{d}{dt}\hat{A}(t) = \frac{i}{\hbar}\left[\hat{H}, \hat{A}(t)\right] + \frac{\partial \hat{A}(t)}{\partial t} \tag{54}$$

where $\hat{H}$ is the Hamiltonian operator. In that picture the quantum fluctuations are characterized by the symmetrized correlation function

$$\begin{aligned} C(\tau) &= \frac{1}{2}\langle \delta\mathbf{F}(0) \cdot \delta\mathbf{F}(\tau) + \delta\mathbf{F}(\tau) \cdot \delta\mathbf{F}(0) \rangle \\ &= \hbar^2 \Omega_R^2 |\langle \chi_2 | \nabla \chi_1 \rangle|^2 \cos(\Omega_R \tau) \end{aligned} \tag{55}$$

with $\delta\mathbf{F}(\tau) = \mathbf{F}(\tau) - \langle \mathbf{F} \rangle$. Dalibard et al. point out that in classical mechanics a particle on which a fast oscillating force $\delta\mathbf{F}$ acts undergoes a micromotion [12]. The average kinetic energy of the particle is then given by

$$E_K = \int \frac{\tilde{C}(\omega)}{2M\omega^2} d\omega, \tag{56}$$

where $\tilde{C}(\omega)$ is the Fourier transform of $C(\tau)$, whose value is inserted in the equation above. One will see that E_K equals the scalar potential W, which arose from the equation for the probability amplitude ψ_1 for finding an atom in the dressed state $|\chi_1\rangle$. From the same equation the vector potential $\mathbf{A}$, which is related to the Berry phase $\gamma(\mathcal{C})$, is obtained. This geometrical phase is added, if a quantum system is slowly encircling the path $\mathcal{C}$ while staying in an eigenstate $|\chi(\mathbf{r})\rangle$ of the particle's Hamiltonian. In *our* case the quantum system contains two energy level states, which can be compared to the atom's or particle's internal degree of freedom. The Berry phase is given by

$$\gamma(\mathcal{C}) = i \oint \langle \chi | \nabla \chi \rangle \cdot d\mathbf{r} = \frac{1}{\hbar} \oint \mathbf{A} \cdot d\mathbf{r}, \tag{57}$$

where second equality holds for the two level system which is prepared in the state $|\chi\rangle$. For a nonzero magnetic field, i.e. $\mathbf{B} = \nabla \times \mathbf{A} \neq 0$, the Lorentz force $\mathbf{F} = \mathbf{v} \times \mathbf{B}$ acts on a particle when it is moving with the velocity $\mathbf{v}$.

Multilevelsystem

In the model systems discussed above the internal state of the particle was a superposition of the ground state $|g\rangle$ and the excited state $|e\rangle$ and both had to have a relatively large weight in order to obtain a non–negligible artificial gauge field. Therefore the lifetime of the excited state $1/\Gamma_e$ has to be relatively long, comparable to alkaline earth

atoms. We will now focus on atoms, whose inner structure corresponds to multilevel systems; this is true for alkali atoms, whose ground state is degenerated and the sublevels are given by $|g_j\rangle$ with $j = 1, ..., N$ as depicted in Fig. 1.

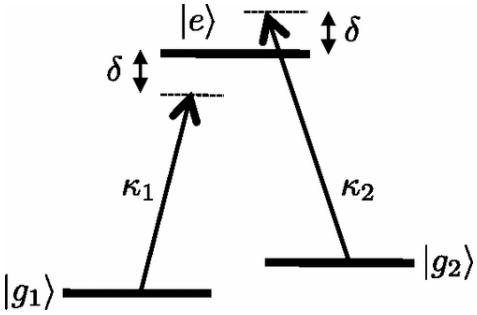

Figure 1: Multilevel atom, with degenerated groundstates $|g_i\rangle_{i=1,2}$ and an excited state $|e\rangle$. δ is the symmetric detuning from the transition frequencies in the Λ structure. κ_1 and κ_2 are the Rabi frequencies. This structure is suitable for a darkstate.

The basis $\{|g_j\rangle\}$ of the ground state manifold is built by the degenerated ground states g_j. In this setting we look for dressed states, which are superpositions of the $|g_j\rangle$ states with negligible involvement of the excited state, $|\chi\rangle \approx \sum_j \alpha_j |g_j\rangle$. This can be achieved by making use of the dark states of – far off the atomic resonance detuned – laser beams. [12, p. 1529.]. An atom prepared in such a dressed state moving with a sufficiently small velocity for adiabatic following will be influenced by the effects of the artificial gauge fields. Because of the use of laser beams suitable for Raman transitions the coefficients α_j can vary strongly on short spatial scale and strong heating caused through spontaneous photon emission must be avoided. Previously we discussed dark states in a Λ scheme, where two ground states $|g_1\rangle$ and $|g_1\rangle$ were coupled via two laser beams to an excited state. The dark state is, like the bright state, an eigenstate of the atom–light field coupling and the former is a linear combination of two ground state levels with *strictly* zero contribution of the excited state. The lasers in a Λ-type atomic level structure is detuned symmetrically in respect to the $|g_1\rangle \to |e\rangle$ and $|g_2\rangle \to |e\rangle$ transition frequencies. The Hamiltonian operator is given by (44) and U the coupling operator between atom and light field is

$$U = \frac{\hbar}{2} \begin{pmatrix} -2\delta & \Omega_1^\star & 0 \\ \Omega_1 & 0 & \Omega_2 \\ 0 & \Omega_2^\star & 2\delta \end{pmatrix} \tag{58}$$

U is written in a basis $\{|g_1\rangle, |e\rangle, |g_2\rangle\}$ using the rotating wave approximation, Ω_1 and Ω_2 denote the complex, space-dependent Rabi frequencies, which include θ and ϕ the two position dependent varying phases and 2δ is the detuning of the two photon process between ground states $|g_1\rangle$ and $|g_2\rangle$.

For a resonant Raman excitation, i.e. $\delta = 0$, the coupling operator U, written in matrix form, has an eigenstate with zero energy called dark or uncoupled [12, p. 1529.]. It reads as

$$|D\rangle = \left(\Omega_2|g_1\rangle - \Omega_1|g_2\rangle\right)/\Omega \tag{59}$$

where $\Omega = \left(|\Omega_1|^2 + |\Omega_2|^2\right)^{1/2}$ and we can see the excited state $|e\rangle$ has no part in the dark state. The other two eigenstates of the coupling operator U are the following $|\pm\rangle = \left(|B\rangle \pm |e\rangle\right)/\sqrt{2}$ with $|B\rangle$ the *bright* (*coupled*) state, which is defined as

$$|B\rangle = \left(\Omega_1^\star|g_1\rangle - \Omega_2^\star|g_2\rangle\right)/\Omega \tag{60}$$

Many groups have studied several phenomena, which depend on the robustness of the dark state $|D\rangle$ regarding decoherence due to sponteanous emission, like stimulated Raman adiabatic passage, subrecoil cooling [2], electromagnetically induced transparency and others.

Since the dressed states $|\chi_j\rangle$ are a complete set of independent states the full atomic state can be written in the form

$$|\Psi(\mathbf{r})\rangle = \sum_{i=D,\pm} \psi_i(\mathbf{r})\,|\chi(\mathbf{r})\rangle \tag{61}$$

where $\psi_D(\mathbf{r})$ and $\psi_\pm(\mathbf{r})$ describe the translational motion of an atom in the internal states $|D(\mathbf{r})\rangle$ and $|\pm(\mathbf{r})\rangle$, respectively. [12, p. 1530.]
Under the assumption of adiabatic approximation, we know the atom will stay in the dark state for the entire time so the full state wave function is reduced to $|\Psi(\mathbf{r})\rangle \approx \psi_D(\mathbf{r})\,|D(\mathbf{r})\rangle$. If one projects the Schrödinger equation on the dark state and neglects coupling to the other internal states $|\pm\rangle$, one obtains the equation of motion for the dark state wave function $\psi_D(\mathbf{r})$, compare (50)

$$i\hbar\frac{\partial\psi_D}{\partial t} = \left[\frac{(\mathbf{P}-\mathbf{A})^2}{2M} + V + W\right]\psi_D \tag{62}$$

where the two geometrical potentials which are spawned by the spatial dependence of the dark state take the forms

$$\mathbf{A} = i\hbar\langle D|\nabla D\rangle \tag{63}$$

and

$$W = \frac{\hbar^2|\langle B|\nabla D\rangle|^2}{2M} \tag{64}$$

By replacing $|\chi_1\rangle$ with $|D\rangle$ and $|\chi_2\rangle$ with $|B\rangle$, we obtain equations similar to (47) and (59). We set

$$\sqrt{\zeta} \equiv \frac{|\Omega_1|}{|\Omega_2|} = -\tan\frac{\theta}{2}, \qquad \phi_1 - \phi_2 = \phi, \tag{65}$$

where the ϕ_j are the phases of the Rabi frequencies $\Omega_j = \tilde{\Omega}_j e^{i\phi_j}$ for $j = 1, 2$. The artificial magnetic field $\mathbf{B} = \nabla \times \mathbf{A}$ in terms of ζ and ϕ is:

$$\mathbf{B} = \hbar \frac{\nabla\phi \times \nabla\zeta}{(1+\zeta)^2} \tag{66}$$

Only if the gradients of the intensity ratio ζ and of the relative phase ϕ are both non zero and not parallel, there is a nonzero effective magnetic field $\mathbf{B}$.

1.5 Superfluidity

If one addresses Bose–Einstein condensation, it is mandatory to discuss also superfluidity. These two phenomena are closely related. A property of a superfluid is that it flows through capillaries and other small structures without dissipating energy and that it possesses no shear viscosity. The first superfluid under experimental investigation was liquid ^4He below the critical λ–point.

Landau's criteria

The theoretical framework of superfluids is based on Galilean transformations of energy and momentum. We are denoting $\mathbf{p}$ and E as the momentum and energy of the fluid in a rest frame. The same quantities $\mathbf{p}'$ and E' of the fluid in the moving frame, whose relative velocity is $\mathbf{v}_{rel}$ with respect to the rest frame have the following form:

$$\mathbf{p}' = \mathbf{p} - m\mathbf{v}_{rel} \tag{67}$$

$$E' \equiv \frac{|\mathbf{p}'|^2}{2m} = \frac{1}{2m}|\mathbf{p} - m\mathbf{v}_{rel}|^2 = E - \mathbf{p}\mathbf{v}_{rel} + \frac{1}{2}m|\mathbf{v}_{rel}|^2, \tag{68}$$

where $E = \frac{|\mathbf{p}|^2}{2m}$ and m the total mass of the fluid.
Assuming the fluid temperature to be $T = 0$ all the particles occupy the ground state and flow in a capillary with a constant $\mathbf{v}$. An inviscous fluid loses its kinetic energy through frictional force with the capillary wall. Such dissipative processes are caused through the creation of an elementary excitation, which is the Bogoliubov quasi particle for an interacting Bose gas.[30, chap 5. p. 2.]
A single excitation with momentum $\mathbf{p}_e$ in the fluid leads to the energy $E_0 + \epsilon(\mathbf{p}_e)$ in the rest frame, which moves with the fluid and the same velocity $\mathbf{v}$. E_0 and $\epsilon(\mathbf{p}_e)$ are the ground state and the elementary excitation energy. In the moving frame the fluid moves with $\mathbf{v}$ but the capillary is at rest. In the moving frame, which moves with velocity $-\mathbf{v}$ in respect to the fluid, the energy and momentum express as follows, if we

set $\mathbf{v}_{rel} = -\mathbf{v}$ and replace $\mathbf{v}_{rel}$ in the momentum and energy definitions above

$$\mathbf{p}' = \mathbf{p}_e - m\mathbf{v} \tag{69}$$

$$E' = E_0 + \epsilon(\mathbf{p}_e) - \mathbf{p}_e\mathbf{v} + \frac{1}{2}m|\mathbf{v}|^2 \tag{70}$$

The above mentioned changes to the energy and the momentum by the elementary excitation are $\epsilon(\mathbf{p}_e) + \mathbf{p}_e \cdot \mathbf{v}$ and $\mathbf{p}_e$.
Spontaneous creation of elementary excitations, i.e. energy dissipation, can occur if and only if such a process is energetically favourable. [30, chap. 5. p. 2.]
This means that dissipation occurs only for the elementary excitation energy $\epsilon(\mathbf{p}_e) + \mathbf{p}_e\mathbf{v}$ smaller than zero. This is true for $|\mathbf{v}| = \epsilon(\mathbf{p}_e)/\mathbf{p}_e$ and $\mathbf{p}_e \cdot \mathbf{v} < 0$, i.e. the fluid velocity and the elementary excitation momentum are oppositely oriented and the fluid velocity must be greater than the critical value given by

$$\mathbf{v}_{cr} = \min_{\mathbf{p}_e} \frac{\epsilon(\mathbf{p}_e)}{\mathbf{p}_e} \tag{71}$$

In compact form the Landau criteria for superfluidity is given by $\mathbf{v}_{rel} < \mathbf{v}_{cr}$, where $\mathbf{v}_{rel}$ is the relative velocity between the capillary wall and the fluid.

1.6 Quantized Vortices

In general vortices imply the breakdown of laminar flow. Fluid rotation can be parametrized by circulation $\Gamma = \oint d\mathbf{r} \cdot \mathbf{v}(\mathbf{r})$ about the vortex, where $\mathbf{v}(\mathbf{r})$ is the velocity field of the fluid. Different from the classical version, superfluids are irrotationals, i.e. $\nabla \times \mathbf{v}(\mathbf{r}) = 0$, and the rotation can only happen through vortices with quantized circulation. Quantized vortices play an important role in the dissipation of transport in superfluids. In BECs these vortices appear in a variety of forms, such as a single vortex, pairs of vortices, rings and vortex lattices. Among others they appear in type–II superconductors.

Quantized Circulation

Under Madelung transformation, the macroscopic condensate wavefunction $\psi(\mathbf{r}, t)$ can be expressed with a fluid density $n(\mathbf{r}, t)$ and a macroscopic phase $S(\mathbf{r}, t)$ via $\psi(\mathbf{r}, t) = \sqrt{n(\mathbf{r}, t)} \exp[iS(\mathbf{r}, t)]$. Quantized vortices can be considered as localized phase singularities. To keep $\psi(\mathbf{r}, t)$ single-valued, the phase change after encircling an closed contour $\mathcal{C}$ must be an integer multiple of 2π [23]

$$\int_{\mathcal{C}} \nabla S \cdot d\mathbf{l} = 2\pi q, \tag{72}$$

where q is an integer. The velocity of the superfluid is defined by $\mathbf{v}_{sf}(\mathbf{r},t) = \frac{\hbar}{m}\nabla S(\mathbf{r},t)$ and based on this the circulation about the closed path $\mathcal{C}$ is given by

$$\Gamma = \int_{\mathcal{C}} \mathbf{v}_{sf} \cdot d\mathbf{l} = q\left(\frac{h}{m}\right) \tag{73}$$

This is the *Onsager Feynman quantisation*. In other words, the circulation of a superfluid is given in discrete units of (h/m). A two dimensional quantized vortex takes the following form

$$\psi(r,\theta) = \sqrt{n_v(r)}\exp(iq\theta). \tag{74}$$

For the vortex density profile $n_v(r)$ there are only approximated solutions and the vortex solution can solely be computed numerically. The vortex consists of a node with zero density. This gap has the width of the condensate healing length $\xi = \hbar/\sqrt{mn_0 g}$, where $g = 4\pi\hbar^2 a_s/m$ and n_0 is the peak density in the undisturbed condensate.[23, p. 3.] The vortex charge q quantifies the rotating direction of the vortex. In case of a vortex with $g = 1$, which is at the center of an axially–symmetric potential, each particle in the vortex carries an angular momentum of $\hbar$. For $q > 1$ the core of the vortex grows due to centrifugal effects. In a condensate in a harmonic trap potential a multiply quantized vortex with $q > 1$ is energetically unfavourable compared to a bunch of single charged vortices, therefore a rotating BEC contains an array of vortices with charge $q = 1$ in the so called triangular Abrikosov lattice form. A multiple quantized vortex can decay in singly–quantized vortices due to dynamical instabilities.

Vortex nucleation

Vortices can originate from different effects like rotation, moving objects or phase imprinting. In case of a rotation a BEC can rotate in presence of quantized vortex lines. The nucleation of the vortex only happens if the rotation frequency exceeds a certain threshold value. For a condensate in an axially–symmetric trapping potential Parker et al. give the critical frequency by [23, p. 4.]

$$\Omega_C = \frac{5}{2}\frac{\hbar}{mR^2}\ln\frac{0.67R}{\xi} \tag{75}$$

This is computed by integrating the kinetic energy density $mn(r)\,v(r)^2/2$ of the vortex velocity field. The lower and upper boundaries are given by the condensate healing length ξ and the Thomas–Fermi radius R. A moving potential presents an alternative way to provoke the nucleation of vortices in BECs. In trapped BECs vortex–anti-vortex pairs can be created by utilizing the optical dipole force by coupling to a laser. A moving localized Gaussian potential gives raise to vortex pairs in numerical simulations, if the

velocity exceeds a certain critical value. In experiments with elongated condensates the vortices could not be observed directly but secondary effects gave evidence for the nucleation of vortices.[17] In another technique called *stirring* the laser beam potential is moved on a circular path to create vortices.

Vortex dynamics

The Helmholtz theorem for uniform, inviscid fluids is also applicable for the dynamics of vortices in super fluids near zero temperature. Its main statement is that the vortex moves along with the background fluid. In the same manner vortices follow the flow of a fluid circulating around a vortex core. Through the presence of other vortices or the curved parts of the vortex line the motion of a vortex can be affected. The velocity of the super fluid $\mathbf{v}_i$ in presence of vortices at the position $\mathbf{r}$ is given by the Biot–Savart law

$$\mathbf{v}_i = \frac{\Gamma}{4\pi} \int \frac{(\mathbf{s} - \mathbf{r}) \times d\mathbf{s}}{|\mathbf{s} - \mathbf{r}|^3}, \tag{76}$$

where $\mathbf{s} = \mathbf{s}(\upsilon, t)$ is a curved path representing the vortex line with υ being the arc length. The assumption for the equation above is that the vortex core is small in comparison to the distance between the vortices. The equation meets its limits if vortices collide, where reconnection events occur. These circumstances must be included manually. Also the divergence at $\mathbf{r} = \mathbf{s}$ deserves special attention. In a system, which inhabits many vortices, the motion of a single vortex and the fluid flow encircling the remaining vortices influence each other. For example two vortices with a charge equally strong but different in sign will move on linear and parallel trajectories and their velocity is inverse proportional to the distance between them.

1.7 Dimensionality and quasi condensates

Until now the properties and effects of Bose gas in three dimensions were discussed. Choosing frequencies of the trapping potential along the three spatial directions which extensively differ from each other constitutes a largely different problem. This leads to disc shaped or two dimensional quasi-condensates or cigar-shaped one-dimensional quasi-condensates. The first fact worth mentioning is that two- and one-dimensional Bose gases show very strange features. Uniform Bose Einstein condensation can not occur in 2D and 1D at temperatures $T > 0$ because thermal fluctuation appear in the condensate and the thermally excited atoms leave the condensate so that the fraction of condensed particles decreases. But in a finite system with repulsive atom–atom interactions, for a temperature sufficiently low, the full phase coherence over the whole cloud is certain[28]. Under the assumption that for an ideal gas in the presence of Bose Einstein condensation the chemical potential $\mu \to 0$, we can see that the momentum

distribution

$$n(\mathbf{p}) \propto \frac{1}{exp(\beta \mathbf{p}^2/2m) - 1}, \qquad \text{with } \beta = 1/k_B T \tag{77}$$

contains an infrared $1/p^2$ divergence [9, p. 471.]. For $N \to \infty, V \to \infty$ and $N/V = const$ emerges a divergent contribution to the integral of the particle distribution $n(\mathbf{p})$ over the whole momentum space in 2D and 1D, which leads to the violation of the demanded normalization of the condensate wave function. For a uniform gas the state density is $\rho(\epsilon) \approx \epsilon^{(d-2)/2}$, where d is the number of dimensions of the space under investigation. For a gas in a harmonic trapping potential the state density behaves like $\sim \epsilon^{d-1}$ and according to Dalfovo et al. [9] the integral in (7) converges in the case $d = 2$. The critical temperature for a two dimensional condensate is given by

$$k_B T_{2D} = \hbar \omega_{2D} \left(\frac{N}{\zeta(2)} \right)^{1/2}, \tag{78}$$

where $\omega_{2D} = (\omega_x \omega_y)^{1/2}$. It must be mentioned that in two dimensions the thermodynamical limit corresponds to taking $N \to \infty$ and $\omega_{2D} \to 0$ with the product $N\omega_{2D}^2$ kept constant. For the experimental realization of two dimensional quasi condensates in real 3D traps, the frequency of the third direction ω_z must be sufficiently large to meet the requirement $\hbar\omega_{2D} \ll k_B T_{2D} < \hbar\omega_z$. For this study the far more interesting situation is the one–dimensional case. According to Dalfovo et al. Bose–Einstein condensation cannot occur even if a harmonic trap potential is used. The reason for this is given by the logarithmic divergence in (7). As a consequence the critical temperature for a 1D Bose–Einstein condensate tends to zero in the thermodynamic limit, if $N\omega_{1D}$ is at a constant value. Ketterle and van Druten gave in [19] an approximation for the critical temperature in an 1D ideal Bose gas. It writes as

$$k_B T_{1D} = \hbar \omega_{1D} \frac{N}{ln(2N)} \tag{79}$$

with $\omega_{1D} \equiv \omega_z$. BECs can not be realized in the thermodynamic limit, but with a finite number N it is possible to realize a system with a large fraction of particles occupying the lowest single particle state in a useful interval of temperatures. Regarding Stimming et al.[28] these temperatures must fulfill the condition of smallness in respect to the energy quantum of the radial Hamiltonian

$$k_B T \ll \hbar \omega_\perp \tag{80}$$

where $\omega_\perp$ is the radial harmonic trap frequency. Another requirement for one–dimensionality, which has to be met, similar to (34), is diluteness, so that the product of the 3D s–wave

scattering length a_s and the mean linear density n_{1D} complies

$$n_{1D} a_s \ll 1. \tag{81}$$

Therefore in uniform systems, where n_{1D} is considered to be constant for all z, with a repulsive, weakly interacting 1D gas, with $g_{1D} > 0$, where the coupling strength is given by $g_{1D} = 2\hbar\omega_\perp a_s$, and at the temperature for one–dimensional quasi–condensation below

$$T_{qc} \sim \frac{\sqrt{g_{1D}\hbar^2 n_{1D}^3/m}}{k_B} \tag{82}$$

the crossover into a phase–coherent state can take place.

2 How to trap and cool atoms

For the experimental realization of Bose-Einstein condensates full integer spin atoms must be cooled down beneath the transition temperature T_C. Without the help of a laser, the main tool for cooling atomic vapours, BEC would not be feasible [24, p. 58ff]. A typical setup for atom vapour cooling can be contrived by the following: A beam of alkali atoms leaves an oven heated to the temperature of 600 K, which corresponds to a mean of the Maxwell-Boltzmann velocity distribution of $\sim 800\ ms^{-1}$. The beam passes through a Zeeman slower, which consists of an inhomogeneous magnetic field and a laser that is counter-propagating to the atomic beam. The radiation force by absorption of photons of the laser beam on the moving alkali atoms slows the photons down. The magnets are designed thus that they annihilate the Doppler effect and the Zeemann effect. The transition frequency can be fixed in the atom's point of view. After passing through the Zeemann slower the atoms move at an approximate velocity of 30 ms^{-1}, which corresponds to 1K.

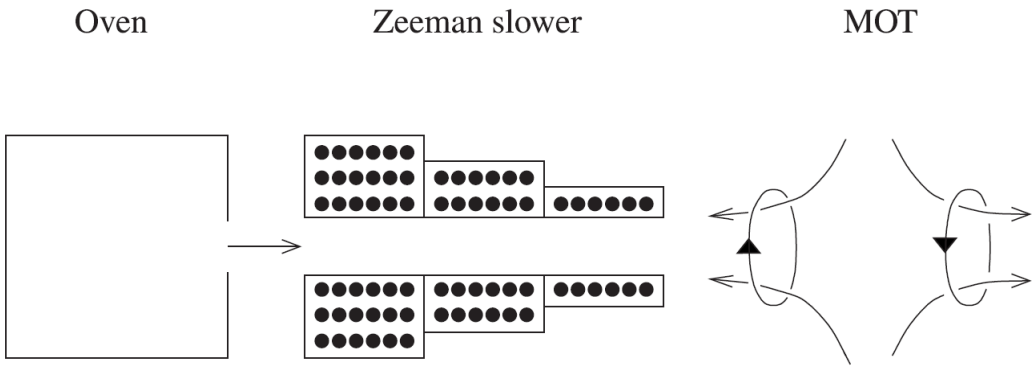

Figure 2: After the oven the atoms are thermal velocity distributed. While passing through the Zeemann–slower the temperature of the atoms is reduced far enough to be loaded into the magneto–optical trap.

Now the alkali atoms are slow i.e. cold enough to be loaded into a magneto optical trap (MOT) to be cooled down further with various techniques.

2.1 Laser cooling

The interactions between atoms and radiation fields, especially the coherent light fields emitted by lasers, are used to implement various cooling and trapping techniques. The interaction between an atomic particle and the electric field is given in the dipole

approximation by

$$H_{IA} = -\mathbf{d} \cdot \mathbf{E} \tag{83}$$

where $\mathbf{d}$ is the electric dipole moment operator and $\mathbf{E}$ is the electric field vector. The change ΔE_g of the ground state energy is of second order in the static electric field and given by

$$\Delta E_g = -\frac{1}{2}\alpha \mathbf{E}^2 \tag{84}$$

where

$$\alpha = 2\sum_e \frac{|\langle e|\mathbf{d}\cdot\hat{\epsilon}|g\rangle|^2}{E_e - E_g} \tag{85}$$

is the atomic polarizability and $\hat{\epsilon}$ is the unit vector with the same direction as the electric field vector $\mathbf{E}$. The time dependent electric field is described by $\mathbf{E}(r,t) = \mathbf{E}_w e^{-i\omega t} + \mathbf{E}_{-\omega} e^{i\omega t}$ with the frequency ω. The condition

$$\mathbf{E}_{-\omega} = \mathbf{E}_{\omega}^* \tag{86}$$

must be fulfilled by the electric field due to the fact that it is real. The first term of $\mathbf{E}(r,t)$ describes the absorption, the second term the emission of a photon in the framework of quantum mechanics. Both parts however do not contribute to the energy shift because

$$\Delta E_g = -\frac{1}{2}\alpha(\omega)\langle \mathbf{E}(r,t)^2\rangle_t \tag{87}$$

where $\langle ...\rangle_t$ is the time average and the dynamical polarizability $\alpha(\omega)$ is given by

$$\alpha(\omega) = \sum_e \frac{2(E_e - E_g)|\langle e|\mathbf{d}\cdot\hat{\epsilon}|g\rangle|^2}{(E_e - E_g)^2 - (\hbar\omega)^2} \tag{88}$$

If the frequency of the radiation field is not detuned far from an atomic resonance a good approximation can be made by neglecting all the other atomic transitions except the resonant one. *Detuning* describes the difference between the frequency of radiation field and the frequency $\omega_{eg} = (E_e - E_g)/\hbar$ of the atomic transition

$$\delta = \omega - \omega_{eg} \tag{89}$$

A positive detuning is termed blue detuning and a negative δ red detuning. The shift of the energy levels is defined by

$$V_g = \frac{\hbar\Omega_R^2\delta}{\delta^2 + \Gamma_e^2/4} \tag{90}$$

The energy shifts are positive for blue and negative for red detuned electric fields respectively. Γ_e is the line width of the excited state, meaning that this state has a life time of $1/\Gamma_e$. Ω_R is the so called Rabi frequency. It describes the oscillation frequency

of an atomic transition under the influence of an electric field $\mathbf{E}_\omega$. It is the magnitude of the perturbing matrix element $|\langle e|\mathbf{d}\cdot\mathbf{E}_\omega|g\rangle|$ and reads as follows

$$\Omega_R = \frac{|\langle e|\mathbf{d}\cdot\mathbf{E}_\omega|g\rangle|}{\hbar} \tag{91}$$

The dressed atom picture describes the atom and its perturbation in the electric field as a single entity. If the time averaged electric field depends on the position, a shift of energy invokes a dipole force.

$$\mathbf{F}_{dipole} = -\nabla V(r) = \frac{1}{2}\alpha'(\omega)\nabla\langle E(r,t)^2\rangle_t \tag{92}$$

Besides the dipole force the radiation force of a radiation field with the wave vector $\mathbf{k}$ plays an important role in cooling atoms.

$$\mathbf{F}_{rad} = \hbar\mathbf{k}\Gamma_g \tag{93}$$

Doppler process

Considering an atom on which two counter propagating laser beams act with the same intensity and frequency ω. Both are slightly red detuned off the transition from ground state $|g\rangle$ to an excited state $|e\rangle$ with the resonance frequency ω_{eg}. The detuning is important to avoid heating by exciting resonances.
Assuming the two laser beams move along the z axis. the absorption rate of a single atom from one beam is given by

$$\frac{dN_\gamma}{dt} = CL(\omega) \tag{94}$$

where

$$C = \frac{\pi}{\hbar^2}|\langle e|\mathbf{d}\cdot\hat{\epsilon}|^2\langle\mathbf{E}(r,t)^2\rangle \tag{95}$$

and L is the Lorentzian function

$$L(\omega) = \frac{\Gamma_e/2\pi}{(\omega-\omega_{eg})^2 + (\Gamma_e/2)^2} \tag{96}$$

Owing to equal absorption of photons from the right as from the left an atom initially at rest, stays at rest, resulting in an overall momentum change of zero. The Doppler effect changes this situation dramatically for a moving atom, since for atoms moving to the right with the velocity v the frequency of the photon moving in the same direction is decreased in its rest frame and is given by, $\omega - vk_\gamma$, where $k_\gamma = \omega/c$ is the wave number. The detuning of the moving atom is larger than for the atom at rest and with

that

$$\frac{dN_r}{dt} = CL\left(\omega - vk_\gamma\right) \tag{97}$$

the photon adsorption rate for the atoms moving to the right is decreased. Moving in the opposite direction, to the left results in different effects as

$$\frac{dN_l}{dt} = CL\left(\omega + vk_\gamma\right) \tag{98}$$

The absorption increases as the left moving atom in its rest frame sees a frequency increased by $\omega + vk_\gamma$. The momentum $\hbar k_\gamma$ transferred during the absorption of photons from the counter-propagating laser beams acts constitutes a friction force on the atom. The transfer rate of momentum is $dp/dt = -\chi v$, where χ is the friction coefficient.[24, p. 75.]

$$\chi \cong 2\hbar k_\gamma C \frac{dL\left(\omega\right)}{d\omega} \tag{99}$$

Assuming the velocity to be such that the Doppler shift is small compared to the line width Γ_e and the detuning δ, the breaking time τ_{fric} determines the momentum loss rate.

$$\frac{1}{\tau_{fric}} = -\frac{1}{p}\frac{dp}{dt} = \frac{\chi}{m} \tag{100}$$

Uncorrelated absorption processes, heating of the atoms and photon emission contributes more or less to a random walk of momentum. (see [24, p. 77.]) The following equation gives the relation between the mean kinetic energy and the temperature for the moving atom

$$\frac{m\bar{v}^2}{2} = k_B T = \hbar L\left(\omega\right)\left(\frac{dL\left(\omega\right)}{d\omega}\right)^{-1} \tag{101}$$

The lowest temperature reachable by Doppler cooling is thus given by

$$k_B T = \frac{\hbar\Gamma_e}{2} \tag{102}$$

The minimum temperature is achieved for a detuning below the resonance frequency by half of the line width of the excited state, which corresponds to red detuning. Blue detuning rather leads to an acceleration than de-acceleration of the atom.
As an example for sodium atoms we consider the linewidth $\Gamma_e \hat{=} 480\mu K$. The minimum temperature after the Doppler process is $\sim 240\mu K$. In the discussion above the atomic cooling was done in one dimension. With six laser beams paired up to form three counter-propagating light fields that intersect in one point, an optical molasses is created, which results in cooling down all three velocity components of the atoms in the cross-section of the laser beams.

[1]

[1] For "Laser Cooling" see Pethick and Smith [24, p. 67ff]

2.2 Magneto Optical Trap

For charged particles techniques like the Penning or the Paul trap can be applied for confinement with the help of magnetic or electrical fields. However for neutral particles the magneto optical trap (MOT) combines a spatially varying magnetic quadrupole field and laser beams to trap neutral atoms in space. Analogue to the Zeemann slower, which was mentioned earlier, the MOT takes advantage of the splitting of the energy levels of the atom into sub-levels in the presence of a magnetic field which is called the Zeemann effect.

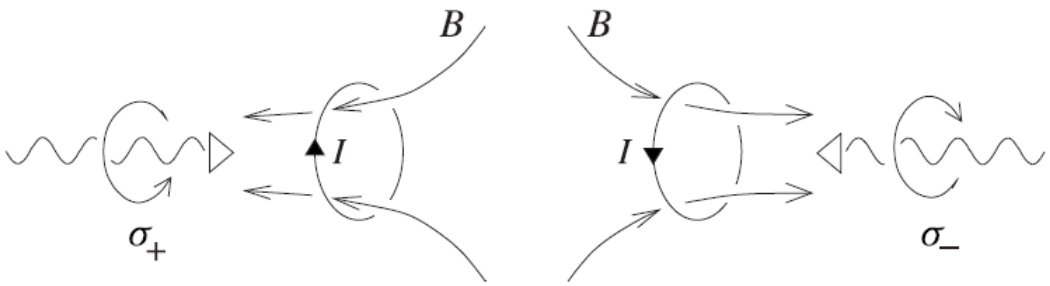

Figure 3: Schematic drawing of the MOT with two counter–propagating, circular polarized laser beams σ_+ and σ_-

Let us consider an atom with a ground state $|g\rangle$ with $J = 0$ and an excited state $|e\rangle$ with $J = 1$, where J is the total angular momentum. As a quantum number the sum of the spin (S) and the orbital angular momentum (L) yields $j = s + l$. The magnetic quantum number m, where $m = -l, -(l-1), ..., -2, -1, 0, 1, 2, ..., (l-1), l$, labels the magnetic sub-states of the excited state and the vector's projection against the z-axis is $m\hbar$. The use of circular polarized laser beams with equal intensity and frequency has the advantage of exciting the atom from the ground state with a non-degenerated magnetic quantum number, therefore levels with $m = 0$, into the $m = +1$ magnetic sub-level, only if it sees the laser beam positive circular polarized (σ_+) and similar into the $m = -1$ sub-level in the case of a σ_- polarized laser beam. Under the assumption of red detuning and for $z = 0$, one can say, that the total momentum transfers from both beams are equal and therefore no overall radiation force acts on the atom. For atoms moving to the right, i.e. $z > 0$ the transition frequency to the $|L = 1, m = -1\rangle$ sub-state is reduced and in consequence the detuning $\delta = \omega - \omega_{m=-1}$ is lowered, while the detuning for the $|L = 1, m = +1\rangle$ sub-state is raised. Furthermore the absorption rate is increased for σ_- photons moving to the left and decreased for σ_+ photons moving to the right. Analogue for displacement to the left with $z < 0$, the absorption rate for σ_+ is higher and the rate for σ_- lower than for $z = 0$.

The simple model described above shows that the MOT not only allows to trap neutral atoms, it is also capable of cooling them effectively with the Doppler process inside the MOT's optical molasses. Due to its inhomogeneous quadrupole magnetic field and the dependence of the atomic frequency on the spatial position the MOT is an effective system to cool atoms with a broad variety of velocities.

In practice limitations of the MOT result from various facts. In general alkali atoms have more than one hyperfine state and as a consequence a process called *optical pumping* takes place, when a fraction of the atoms is, by a resonant laser, raised into a different excited state than the targeted one. From this non-resonant energy level the atoms can decay into the initial or a completely different ground state level, which is unreachable for the light field. Therefore these are called *dark states*, whereas the *bright states* inhabit the transition the MOT is tuned to. If the bright state population is depleted too much, the MOT will cease to work.
The terminus *repumping* describes the use of a laser resonant to the transition from the dark state to the falsely excited level. The atoms are repumped to the exited state and have a certain probability to decay into the initial ground state level and therefore increase the bright state's population.

[2]

2.3 Evaporative cooling

Laser cooling does not suffice to achieve a condensation of the atom gas. The next step closer to the transition temperature T_C for Bose-Einstein condensation is called *evaporative cooling*. It uses the fact that particles with higher than average energy leave the system and the remaining particles stay in the system, but with their temperature lowered, as can be seen in Fig 4. Assuming that all the atoms own the same energy $\bar{\epsilon}$, results in the evaporated particles having, with $(1+\beta)\,\hat{\epsilon}$ an energy higher than the average. If we call the particles number change dN, then the energy loss trough evaporative cooling is $(1+\beta)\,\hat{\epsilon}dN$. By energy conservation the total energy of the particles inside the trap is $E + (1+\beta)\,\hat{\epsilon}dN$ and the number of remaining particles $N + dN$. The quotient of these two values yields the average energy of the remaining atoms

$$\bar{\epsilon} + d\bar{\epsilon} = \frac{E + (1+\beta)\,\bar{\epsilon}dN}{N + dN} \tag{103}$$

and

$$\frac{d\ln\bar{\epsilon}}{d\ln N} = \beta \tag{104}$$

[2]For "Magneto Optical Trap" see Pethick and Smith [24, p. 78ff]

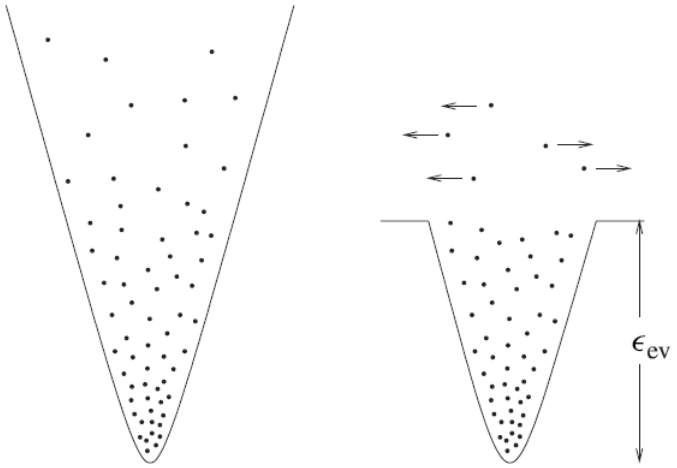

Figure 4: The thermal cloud in the potential contains particles with all classes of velocities. From the lowered potential the *hotter* atoms with energy higher than ϵ_{ev} can escape and the remaining ensemble of atoms is cooled down

If β is independent of the particle number N then

$$\frac{\hat{\epsilon}}{\hat{\epsilon}_0} = \left(\frac{N}{N_0}\right)^{\beta} \tag{105}$$

where $\hat{\epsilon}_0 = \hat{\epsilon}\,(0)$ and $N_0 = N\,(0)$ are initial conditions. From the last relation above out of a simplified model for evaporative cooling one can see, that the average energy of the remaining gas particles decline for a decreasing number of particle N. Regarding to Pethick and Smith in [24, p. 92.] the relation between averaged energy $\hat{\epsilon}$ and the temperature T depends on the trap potential. Their consideration for simple results are potentials, which are homogeneous functions of the coordinates to the power of ν

$$V\,(\mathbf{r}) = \alpha\,(\hat{\mathbf{r}})\,r^{\nu} \tag{106}$$

where $\alpha\,(\hat{\mathbf{r}})$ is a possibly direction depending coefficient. For an ideal gas one can show that [24, p. 92.]

$$2\bar{\epsilon}_{kin} = \frac{3}{d}\nu\overline{V} \tag{107}$$

where ϵ_{kin} is the kinetic energy of the particle and V is the trapping potential. The bar denotes a thermal average, which for a given quantity or observable A is defined by

$$\langle A\rangle = \frac{\sum_i A e^{-E_i/k_BT}}{\sum_i e^{-E_i/k_BT}} \tag{108}$$

and is often referred to as Boltzmann average. It depicts the expectation value of the investigated property at a given temperature T. Throughout most of the evaporation cooling process effects caused by quantum degeneracies are negligible, so we can use

an ideal gas approximation. The kinetic energy averaged is correspondingly

$$\bar{\epsilon}_{kin} = \frac{3}{2} k_B T \tag{109}$$

and, for that matter, the average energy per particle $\bar{\epsilon}$

$$\bar{\epsilon} = \left(\frac{3}{2} + \frac{d}{\nu} \right) k_B T \tag{110}$$

From this it is apparent that the temperature of the gas is also dependent on the particle number as is the average energy

$$\frac{d \ln T}{d \ln N} = \beta \tag{111}$$

From (104) and (111) we can see that the change of the average energy of the remaining particles and change of temperature both depend on the change of the number of the remaining particles, i.e. if high energy particles are evaporated, the descent of the temperature steepens due to loss of a certain number of particles, but other effects like inter-atomic elastic collisions can lead to a lowered evaporation rate.

[3]

[3] For "Evaporative Cooling" see Pethick and Smith [24, p. 90ff]

3 Numerical models and methods

3.1 Gross–Pitaevskii equation: Standard model for BEC

The non-linear Schrödinger equation, called Gross–Pitaevskii equation, has been used to describe the Bose Einstein condensate in the meanfield approach. Only few experiments in ultra-cold dilute Bose gas did not meet the theoretical predictions calculated from the GPE [4, p. 1674.]. A series of studies used the time-independent GPE to find the ground states numerically and the time–dependent GPE to illustrate the dynamics of a variety of BECs with varois shapes and in different dimensions. Many different numerical methods are applied, but every ansatz leads back to the same fundamental problem, namely computational simulations of a Bose Einstein condensate in the ground state.
The non-linear Schrödinger equation is

$$i\psi_t = -\frac{1}{2}\Delta\psi + V(\mathbf{x})\,\psi + \beta|\psi|^2\psi, \qquad t > 0, \mathbf{x} \in \Omega \subseteq \mathbb{R}^d \tag{112}$$

$$\psi(\mathbf{x}, t) = 0, \qquad \mathbf{x} \in \Gamma = \partial\Omega, \quad t \geq 0, \qquad \phi(\mathbf{x}, 0) = \phi_0(\mathbf{x}), \qquad \mathbf{x} \in \Omega \tag{113}$$

where Ω is a subspace of $\mathbb{R}^d$ and $\partial\Omega$ the boundary of Ω. For a defocusing or focusing non-linear Scrödinger equation respectively, the value of β is positive or negative. The shape of the studied BEC determines the shape of the real valued potential $V(\mathbf{x})$. The solution of the Gross–Pitaevskii equation ψ describes the condensate's wave function and its macroscopic behaviour. Here t is the time coordinate, $\mathbf{x}$ the position in space and $V(\mathbf{x})$ the trapping potential, which in the most cases is harmonic and therefore takes the form

$$V(\mathbf{x}) = \frac{1}{2}\left(\gamma_1^2 x_1^2 + ... + \gamma_d^2 x_d^2\right) \tag{114}$$

with $\gamma_1, ..., \gamma_d > 0$. The BEC wave function has to be normalized by the condition

$$N(\psi) = \int_\Omega |\psi(\mathbf{x}, t)|^2 d\mathbf{x} = 1, \quad t \geq 0 \tag{115}$$

and the associated energy is

$$E_\beta(\psi) = \int_\Omega \left[\frac{1}{2}\nabla|\psi(\mathbf{x}, t)|^2 + V(\mathbf{x})\,|\psi(\mathbf{x}, t)|^2 + \frac{\beta}{2}|\psi(\mathbf{x}, t)|^4\right] d\mathbf{x}, \quad t \geq 0. \tag{116}$$

For the stationary solution we expand the separable function $\psi(\mathbf{x}, t)$ to

$$\psi(\mathbf{x}, t) = e^{-i\mu t}\phi(\mathbf{x}), \tag{117}$$

where μ is again the chemical potential and ϕ is a time independent, real valued

function. This leads to the following equation

$$\mu\phi\left(\mathbf{x}\right)=-\frac{1}{2}\Delta\phi\left(\mathbf{x}\right)+V\left(\mathbf{x}\right)\phi\left(\mathbf{x}\right)+\beta|\phi\left(\mathbf{x}\right)|^{2}\phi\left(\mathbf{x}\right),\qquad x\in\Omega \tag{118}$$

under the constraint

$$\phi\left(\mathbf{x}\right)=0,\quad \mathbf{x}\in\Gamma. \tag{119}$$

ϕ is normalized under

$$\int_{\Omega}|\phi\left(\mathbf{x}\right)|^{2}d\mathbf{x}=1. \tag{120}$$

This is a non-linear eigenvalue problem with the eigenvalue μ and the eigenfunctions ϕ. Any μ takes for its eigenfunction ϕ the following form

$$\mu_{\beta}\left(\phi\right)=\int_{\Omega}\left[\frac{1}{2}\nabla|\phi\left(\mathbf{x}\right)|^{2}+V\left(\mathbf{x}\right)|\phi\left(\mathbf{x}\right)|^{2}+\beta|\phi\left(\mathbf{x}\right)|^{4}\right]d\mathbf{x} \tag{121}$$

$$=E_{\beta}\left(\phi\right)+\int_{\Omega}\frac{\beta}{2}|\phi\left(\mathbf{x}\right)|^{4}d\mathbf{x}. \tag{122}$$

Gradient flow with discrete normalization

In order to find the ground state solution $\phi_g\left(\mathbf{x}\right)$ of equation (118), a real and positive function, the energy has to be minimized. A popular technique to work with the normalization constraint (120) is to choose a time sequence as $0=t_0<t_1<t_2<...<t_n<...$ with $\Delta t_n=t_{n+1}-t_n>0$ and $k=max_{n\geq 0}\Delta t_n$. The following imaginary time propagation (see **4.1**) can be used for computing the ground state solution of BECs [4, p. 1676.]

$$\phi_t=-\frac{1}{2}\frac{\delta E_{\beta}\left(\phi\right)}{\delta\phi}=\frac{1}{2}\Delta\phi-V\left(\mathbf{x}\right)\phi-\beta|\phi|^{2}\phi,\quad \mathbf{x}\in\Omega,t_n<t<t_{n+1},n\geq 0, \tag{123}$$

$$\phi\left(\mathbf{x},t_{n+1}\right)\triangleq\phi\left(\mathbf{x},t_{n+1}^{+}\right)=\frac{\phi\left(\mathbf{x},t_{n+1}^{-}\right)}{||\phi\left(\cdot,t_{n+1}^{-}\right)||},\quad \mathbf{x}\in\Omega,n\geq 0, \tag{124}$$

$$\phi\left(\mathbf{x},t\right)=0,\quad \mathbf{x}\in\Gamma,\qquad \phi\left(\mathbf{x},0\right)=\phi_0\left(\mathbf{x}\right),\quad \mathbf{x}\in\Omega \tag{125}$$

where $\phi\left(\mathbf{x},t_n^{\pm}\right)=\lim_{t\to t_n^{\pm}}\phi\left(\mathbf{x},t\right)$ and $||\phi_0||=1$. Here we set $||\cdot||$ as the norm of the quadratically integrable function $||\cdot||_{L^2(\Omega)}$ over the subset Ω of $\mathbb{R}^d$. The gradient flow corresponds to the steepest descent method to the energy functional $E_{\beta}\left(\phi\right)$ without the constraint (120). Then (124) projects the solution onto a unit sphere obeying the constraint, i.e. the normalization of the wave function.

To demonstrate the energy minimizing property of this algorithm first we define

$$\bar{\phi}\left(\cdot,t\right)=\frac{\phi\left(\cdot,t\right)}{||\phi\left(\cdot,t\right)||}\quad\text{for}\quad t_n\leq t\leq t_{n+1}\quad\text{and}\quad n\geq 0. \tag{126}$$

Bao and Du state in [4] under the assumptions $V(\mathbf{x}) \geq 0$ for all $\mathbf{x} \in \Omega$, $\beta \leq 0$ and $||\phi_0|| = 1$, that the following is true

$$i) \qquad ||\phi(\cdot,t)|| \;\leq\; ||\phi(\cdot,t_n)|| = 1 \text{ for } t_n \leq t \leq t_{n+1},\ n \geq 0; \tag{127}$$

$$ii) \qquad E_\beta(\phi(\cdot,t)) \leq E_\beta\left(\phi\left(\cdot,\tilde{t}\right)\right), \quad t_n \leq \tilde{t} \leq t_{n+1},\ n \geq 0, \quad \forall\ \beta \geq 0; \tag{128}$$

$$iii) \qquad E_0\left(\bar{\phi}(\cdot,t)\right) \leq\ E_0\left(\bar{\phi}(\cdot,t_n)\right), \quad t_n \leq t \leq t_{n+1},\ n \geq 0,\ \text{for } \beta = 0; \tag{129}$$

and that for $V(\mathbf{x})\ \forall\ \mathbf{x} \in \Omega$ and $||\phi_0|| = 1$ the gradient flow with discrete normalization diminishes the energy for any time step k and initial data ϕ_0 [4, p. 1677.], i.e.

$$E_0(\phi(\cdot,t_{n+1})) \leq E_0(\phi(\cdot,t_n)) \leq ... \leq E_0(\phi(\cdot,0)) = E_0(\phi_0), \qquad n = 0,1,2,.... \tag{130}$$

Continuous normalized gradient flow

The normalization step (124) corresponds to solving the following ordinary differential equation exactly

$$\phi_t(\mathbf{x},t) = \mu_\phi(t,k)\,\phi(\mathbf{x},t), \qquad \mathbf{x} \in \Omega,\ t_n < t < t_{n+1},\ n \geq 0 \tag{131}$$

$$\phi\left(\mathbf{x},t_n^+\right) = \phi\left(\mathbf{x},t_{n+1}^-\right), \quad \mathbf{x} \in \Omega \tag{132}$$

The term $\mu_\phi(t,k)$ takes the form

$$\mu_\phi(t,k) \equiv \mu_\phi(t_{n+1},\Delta t_n) = -\frac{1}{2\Delta t_n} ln||\phi\left(\cdot,t_{n+1}^-\right)||^2, \qquad t_n \leq t \leq t_{n+1}. \tag{133}$$

Therefore the gradient flow with discrete normalization can be viewed as splitting method of 1^{st} order for the flow with discontinuous coefficients:

$$\phi_t = \frac{1}{2}\Delta\phi - V(\mathbf{x})\,\phi - \beta|\phi|^2\phi + \mu_\phi(t,k)\,\phi, \quad \mathbf{x} \in \Omega, t \geq 0, \tag{134}$$

$$\phi(\mathbf{x},t) = 0, \quad \mathbf{x} \in \Gamma, \qquad \phi(\mathbf{x},0) = \phi_0(\mathbf{x}), \quad \mathbf{x} \in \Omega. \tag{135}$$

In the limit $\mu_\phi(t)$ is

$$\lim_{k\to 0}\mu_\phi(t,k) = \mu_\phi(t) = \frac{1}{||\phi(\cdot,t)||^2}\int_\Omega\left[\frac{1}{2}|\nabla\phi(\mathbf{x},t)|^2 + V(\mathbf{x})\,\phi^2(\mathbf{x}) + \beta\phi^4(\mathbf{x})\right]d\mathbf{x} \tag{136}$$

and as a consequence from the above the following continuous normalized gradient flow should be taken into consideration

$$\phi_t = \frac{1}{2}\Delta\phi - V(\mathbf{x})\,\phi - \beta|\phi|^2\phi + \mu_\phi(t)\,\phi, \quad \mathbf{x} \in \Omega, t \geq 0, \tag{137}$$

$$\phi(\mathbf{x},t) = 0, \quad \mathbf{x} \in \Gamma, \qquad \phi(\mathbf{x},0) = \phi_0(\mathbf{x}), \quad \mathbf{x} \in \Omega. \tag{138}$$

If one takes $\mu_\phi(t)$ on the right side of (137) as a Lagrange multiplier for the constraint (120), we arrive at the result that (137) and (118) are identical in case of a stationary ϕ in (137).

The full time discretization our initial scheme is the following semi–implicit time discretization

$$\frac{\bar{\phi}^{n+1}-\phi^n}{k}=\frac{1}{2}\Delta\bar{\phi}^{n+1}-V(\mathbf{x})\,\bar{\phi}^{n+1}-\beta|\phi^n|^2\bar{\phi}^{n+1},\quad \mathbf{x}\in\Omega \tag{139}$$

$$\bar{\phi}^{n+1}(\mathbf{x})=0,\quad \mathbf{x}\in\Gamma,\qquad \phi^{n+1}(\mathbf{x})=\frac{\bar{\phi}^{n+1}(\mathbf{x})}{||\bar{\phi}^{n+1}||},\quad \mathbf{x}\in\Omega \tag{140}$$

This can be seen as a discretization of a linear gradient flow with a modified potential

$$\tilde{V}(\mathbf{x})=V(\mathbf{x})+\beta|\phi^n(\mathbf{x})|^2 \tag{141}$$

Time–splitting sine–spectral method

The time splitting method is used to solve the equation (123). During one time step from $t=t_n$ to $t=t_{n+1}$ the equation

$$\phi_t=\frac{1}{2}\phi_{xx}-V(x)\,\phi-\beta|\phi|^2\phi,\quad x\in\Omega=(a,b),\ t_n<t<t_{n+1},\ n\geq 0 \tag{142}$$

is solved in two stages. The first one is to solve the linear partial differential equation of second order

$$\phi_t=\frac{1}{2}\phi_{xx}. \tag{143}$$

for one time step of the length $k=t_{n+1}-t_n$. One has to solve the differential equation

$$\phi_t(x,t)=-V(x)\,\phi(x,t)-\beta|\phi|^2\phi(x,t),\qquad t_n\leq t\leq t_{n+1} \tag{144}$$

for the same time step from t_n to t_{n+1}. The spatial coordinate is discretized in (143) by the sine–spectral method. The differential equation of the first step can be integrated in time exactly. For $t\in[t_n,t_{n+1}]$, multiplying the ordinary differential equation from the second stage with $\phi(x,yt)$, one obtains $\rho(x,t)=\phi^2(x,t)$.[4, p. 1683.]

$$\rho_t(x,t)=-2V(x)\,\rho(x,t)-2\beta\rho^2(x,t),\qquad t_n\leq t\leq t_{n+1} \tag{145}$$

The solution of the ordinary differential equation above can be written as

$$\rho(x,t)=\begin{cases}\frac{V(x)\rho(x,t_n)}{(V(x)+\beta\rho(x,t_n))e^{2V(x)(t-t_n)}-\beta\rho(x,t_n)} & V(x)\neq 0,\\ \frac{\rho(x,t_n)}{1+2\beta\rho(x,t_n)(t-t_n)} & V(x)=0.\end{cases} \tag{146}$$

To compute the disϕ_j^{n+1} from the previous ϕ_j^n one has to consider these following steps

$$\phi_j^\star = \begin{cases} \sqrt{\frac{V(x_j)e^{-kV\left(x_j\right)}}{V(x_j)+\beta\left(1-e^{-kV\left(x_j\right)}\right)|\phi_j^n|^2}}\phi_j^n, & V\left(x_j\right) \neq 0, \\ \frac{1}{\sqrt{1+\beta|\phi_j^n|^2}}\phi_j^n, & V\left(x_j\right) = 0. \end{cases} \tag{147}$$

$$\phi_j^{\star\star} = \sum_{l=1}^{M-1} e^{-k\mu_l^2/2}\hat{\phi_l^\star}\sin\left(\mu_l\left(x_j-a\right)\right), \qquad j=1,2,...,M-1 \tag{148}$$

$$\phi_j^{\star\star\star} = \begin{cases} \sqrt{\frac{V(x_j)e^{-kV\left(x_j\right)}}{V(x_j)+\beta\left(1-e^{-kV\left(x_j\right)}\right)|\phi_j^{\star\star}|^2}}\phi_j^{\star\star}, & V\left(x_j\right) \neq 0, \\ \frac{1}{\sqrt{1+\beta|\phi_j^{\star\star}|^2}}\phi_j^{\star\star}, & V\left(x_j\right) = 0. \end{cases} \tag{149}$$

$$\phi_j^{n+1} = \frac{\phi_j^{\star\star\star}}{||\phi_j^{\star\star\star}||}, \qquad j=0,...,M.\ n=0,1,..., \tag{150}$$

where $\hat{U}_l$ are the sine transformed coefficients of $U = (u_0, u_1, ..., u_M)$ with $u_i \in \mathbb{R}\ \forall\ i = 0, ..., M$ and $u_0 = u_M = 0$. They are defined as

$$\mu_l = \frac{\pi l}{b-a}, \qquad \hat{U}_l = \frac{2}{M}\sum_{j=1}^{M-1} u_j \sin\left(\mu_j\left(x_j-a\right)\right), \qquad l=1,2,...,M-1 \tag{151}$$

and

$$\phi_j^0 = \phi\left(x_l,0\right) = \phi_0\left(x_j\right), \qquad j=0,1,2,...,M. \tag{152}$$

[4]

[4]For chapter 3 "Time Splitting Spectral Method" see Bao and Du [4]

4 Two coupled 1–d Bose Einstein condensates

The phase transitions, marking the crossing of a system between two phases accompanied by severe macroscopic behaviour changes, are driven by thermal fluctuations. At temperatures $T \to 0$ the thermal fluctuations freeze out, but their quantum mechanical counter parts, the quantum fluctuations, are still present. While for classical systems a $T = 0$ phase transition is impossible, for quantum systems Heisenberg's uncertainty relation allows fluctuations and thereby phase transitions.[16] The main topic of this study was to find a quantum phase transition in two one–dimensional Bose–Einstein condensates in their ground states, when an artificial gauge field is applied. As said before, several methods of imprinting such an artificial magnetic field onto neutral atoms exist. It can be obtained by a laser field, microwaves or a radio–frequency field. Through an additional kinetic term caused by the artificial gauge field the particles begin to migrate inside the elongated Bose–Einstein condensates. Since the two quasi condensates are in close proximity, probability for tunnelling has to be accounted for. Thus, quantum vortices are expected to emerge. The pictorial schematic in Fig. 5 shows the basic idea of the investigated system.

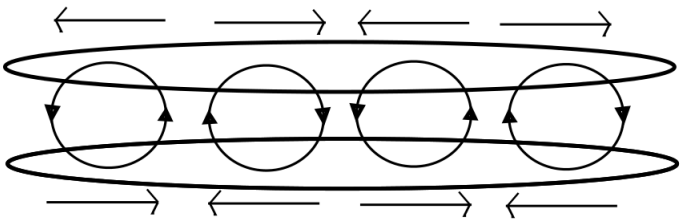

Figure 5: The two elliptical objects represent the cigar shaped one dimensional BECs, which are aligned along the z–axis. The arrows above and below correspond to the directions in which the atoms inside the BECs are moving. The circles represent the expected vortices, whereas the small arrows on the circle indicate the charge carried by the vortices.

Resulting from all the assumptions made above we obtain a system of coupled differential equations. They are second order, non-linear partial differential equations. The two modified GPEs with $\psi_i = \psi_i(z,t)$, for $i = 1, 2$ write as

$$i\hbar\frac{\partial}{\partial t}\psi_1 = -\frac{\hbar^2}{2m}\left(\partial_z - ik_0\right)^2\psi_1 + g|\psi_1|^2\psi_1 + \frac{m\omega_{\shortparallel}z^2}{2}\psi_1 - \hbar J\psi_2 \tag{153}$$

$$i\hbar\frac{\partial}{\partial t}\psi_2 = -\frac{\hbar^2}{2m}\left(\partial_z + ik_0\right)^2\psi_2 + g|\psi_2|^2\psi_2 + \frac{m\omega_{\shortparallel}z^2}{2}\psi_2 - \hbar J\psi_1, \tag{154}$$

with

$$g = \frac{4\pi\hbar^2 a_s}{m}, \tag{155}$$

where a_s is the s–wave scattering length and g determines the interactions between

atoms in the condensate. For $g > 0$ there is a repulsive force, for $g < 0$ an attractive force. The factor k_0 describes the contribution of the artificial gauge field. This corresponds to the $(\mathbf{P} - \mathbf{A})$ term in the equations (50) and (62) in the artificial gauge field discussed in the previous section. The $\omega_{\shortparallel}$ in the potential term is the frequency of the trap along the z–axis. J is the coefficient of the tunnelling matrix, which couples the two one–dimensional BECs.

4.1 Imaginary time propagation

One obtains the time evolution of the wave functions of the BECs by applying $U = exp\left[-iHt/\hbar\right]$ the unitary time evolution operator on the the wave-function $\psi_i\left(z,0\right)$ for $i = 1, 2$. For both wave functions written in vector form the time evolution can be calculated as

$$\left.\begin{pmatrix}\psi_1\\ \psi_2\end{pmatrix}\right|_t = e^{-\frac{iHt}{\hbar}} \left.\begin{pmatrix}\psi_1\\ \psi_2\end{pmatrix}\right|_{t=0} \tag{156}$$

where H is the Hamiltonian of our investigated system. It is a hermitian operator, that means $H = H^\dagger$ or $HH^\dagger = \mathbb{1} = H^\dagger H$, where $\mathbb{1}$ is the identity operator. Another property of the hermitian operator is the possession of only real eigenvalues and that the real eigenfunctions construct the basis for the Hilbert space.
If one takes advantage of the separability of the Hamiltonian, one can write the Hamiltonian operator in the form

$$H = |0\rangle\langle 0|\epsilon_0 + |1\rangle\langle 1|\epsilon_1 + ... \tag{157}$$

where $|0\rangle, |1\rangle, |2\rangle, ...$ are the eigenfunctions of the Hamiltonian and $\epsilon_0, \epsilon_1, \epsilon_2, ...$ the associated eigenvalues or the eigenenergy levels respectively and $\epsilon_0 = min\left(\epsilon_i\right)$. The items $|n\rangle\langle n|$ for $n = 0, 1, 2, ...$ represent the projector onto the n^{th} subspace. The exponential operator U can be expanded in the form

$$e^{-\frac{iHt}{\hbar}} = |0\rangle\langle 0|e^{-\frac{t\epsilon_0 t}{\hbar}} + |1\rangle\langle 1|e^{-\frac{i\epsilon_1 t}{\hbar}} + ... \tag{158}$$

With $t = -i\tau$, where τ is the imaginary time the evolution operator takes the form

$$e^{-\frac{H\tau}{\hbar}} = |0\rangle\langle 0|e^{-\frac{\epsilon_0 \tau}{\hbar}} + |1\rangle\langle 1|e^{-\frac{\epsilon_1 \tau}{\hbar}} + ... \tag{159}$$

and the development of the wave functions of the two tunnel–coupled BECs is written as follows:

$$\left.\begin{pmatrix}\psi_1\\ \psi_2\end{pmatrix}\right|_\tau = e^{-\frac{H\tau}{\hbar}} \left.\begin{pmatrix}\psi_1\\ \psi_2\end{pmatrix}\right|_{\tau=0} \tag{160}$$

Imaginary time propagation method makes use of the separability of the Hamiltonian operator and therefore the problem can be solved by applying a splitting method. A frequently used approach for solving this kind of problem is to introduce an imaginary time ($t = -i\tau$). The solution arises from what can be called the imaginary time evolution exponential operator $U_\tau = \exp\left(-\tau \hat{H}\right)$. If one wants to compute the solution, one will see that any set of initial conditions $\psi_i|_{\tau=0}$, which are under the action of U_τ, converge asymptotically towards the ground state solution for $\tau \to \infty$. The imaginary evolution operator has with $U_\tau = \exp\left(-\tau \hat{H}\right)$ the same eigenfunctions as the initial problem. In the technique called imaginary time propagation only the action of $\exp\left(-\tau \hat{H}\right)$ on the condensate's wave–functions has to be computed.[3]

By setting $t = -i\tau$ and $\partial t = -i\partial\tau$ the two coupled differential equations become

$$-\hbar\frac{\partial}{\partial\tau}\psi_1 = -\frac{\hbar^2}{2m}\left(\partial_z - ik_0\right)^2\psi_1 + g|\psi_1|^2\psi_1 + \frac{m\omega_{\shortparallel}z^2}{2}\psi_1 - \hbar J\psi_2 \tag{161}$$

$$-\hbar\frac{\partial}{\partial\tau}\psi_2 = -\frac{\hbar^2}{2m}\left(\partial_z + ik_0\right)^2\psi_2) + g|\psi_2|^2\psi_2 + \frac{m\omega_{\shortparallel}z^2}{2}\psi_2 - \hbar J\psi_1 \tag{162}$$

with $\psi_i = \psi_i\left(z,\tau\right)$ for $i = 1, 2$. The two wave-functions, which are solving our system of differential equations have to be properly normalized:

$$\int_{-\infty}^{\infty} dz|\psi_1\left(z,\tau\right)|^2 = \int_{-\infty}^{\infty} dz|\psi_2\left(z,\tau\right)|^2 = N, \tag{163}$$

where N is number of particles in the condensate.

4.2 Dimensionless GPE

In order to scale the two equations (161) and (162), we introduce the following relations:

$$\bar{\tau} = \omega_{\shortparallel}\tau \tag{164}$$

$$g = 2\hbar\omega_{\perp}a_s \tag{165}$$

$$l_0 = \sqrt{\frac{\hbar}{m\omega_{\shortparallel}}} \tag{166}$$

$$\bar{z} = \sqrt{\frac{m\omega_{\shortparallel}}{\hbar}}z, \tag{167}$$

where l_0 is the harmonic oscillator length, $\omega_{\perp}$ the trap frequency in the $x-y$ plane and $\omega_{\shortparallel}$ the trap frequency along the z–axis. Plugging this into (161) and (162) gives the dimensionless version of our tunnel–coupled GPEs, where ψ_i is from now on $\psi_i = \psi_i\left(\bar{z},\bar{\tau}\right)$, for $i = 1, 2$,

$$-\frac{\partial}{\partial\bar{\tau}}\psi_1 = -\frac{1}{2}\left(\frac{\partial}{\partial\bar{z}} - ik_0l_0\right)^2\psi_1 + \frac{2\omega_{\perp}a_s}{\omega_{\shortparallel}}|\psi_1|^2\psi_1 + \frac{1}{2}\bar{z}^2\psi_1 - \frac{J}{\omega_{\shortparallel}}\psi_2 \tag{168}$$

$$-\frac{\partial}{\partial\bar{\tau}}\psi_2 = -\frac{1}{2}\left(\frac{\partial}{\partial\bar{z}} + ik_0 l_0\right)^2 \psi_2 + \frac{2\omega_\perp a_s}{\omega_{\shortparallel}}|\psi_2|^2\psi_2 + \frac{1}{2}\bar{z}^2\psi_2 - \frac{J}{\omega_{\shortparallel}}\psi_1 \tag{169}$$

In the same manner the rescaling relations are applied to the normalization conditions for the two wave–functions $\psi_1(\bar{z},\bar{\tau})$ and $\psi_2(\bar{z},\bar{\tau})$,

$$\int_{-\infty}^{\infty} dz|\psi_1|^2 = l_0\int_{-\infty}^{\infty} d\bar{z}|\psi_1|^2 = N \tag{170}$$

where N is the number of particles. From this we get

$$\psi_1 = \frac{\sqrt{N}\bar{\psi}_1}{\sqrt{l_0}} \qquad \text{and} \qquad \psi_2 = \frac{\sqrt{N}\bar{\psi}_2}{\sqrt{l_0}} \tag{171}$$

which finally leads to the new normalization conditions for $\bar{\psi}_1$ and $\bar{\psi}_2$,

$$\int_{-\infty}^{\infty} d\bar{z}|\bar{\psi}_1|^2 = 1 \quad \text{respectively} \quad \int_{-\infty}^{\infty} d\bar{z}|\bar{\psi}_2|^2 = 1. \tag{172}$$

Two further substitutions, namely $\bar{J} = J/\omega_{\shortparallel}$ and $\bar{k} = k_0\, l_0$ leave us with the two dimensionless, coupled equations describing the dynamics of two tunnel–coupled 1D BECs:

$$-\frac{\partial}{\partial\bar{\tau}}\bar{\psi}_1 = -\frac{1}{2}\left(\frac{\partial}{\partial\bar{z}} - i\bar{k}\right)^2 \bar{\psi}_1 + \frac{2\omega_\perp}{\omega_{\shortparallel}}\frac{a_s}{l_0}N|\bar{\psi}_1|^2\bar{\psi}_1 + \frac{1}{2}\bar{z}^2\bar{\psi}_1 - \bar{J}\bar{\psi}_2 \tag{173}$$

$$-\frac{\partial}{\partial\bar{\tau}}\bar{\psi}_2 = -\frac{1}{2}\left(\frac{\partial}{\partial\bar{z}} + i\bar{k}\right)^2 \bar{\psi}_2 + \frac{2\omega_\perp}{\omega_{\shortparallel}}\frac{a_s}{l_0}N|\bar{\psi}_2|^2\bar{\psi}_2 + \frac{1}{2}\bar{z}^2\bar{\psi}_2 - \bar{J}\bar{\psi}_1 \tag{174}$$

where $\bar{\psi}_i = \bar{\psi}_i(\bar{z},\bar{\tau})$, for $i = 1, 2$.
For $\bar{J} = 0$ and $\bar{k} = 0$ and $\left(\frac{\partial}{\partial\bar{z}}\right)^2 \to 0$ we obtain the following relation

$$\frac{m\omega^2}{2}z^2 + gn(z) = gn_0 \tag{175}$$

which leads to the density profile below

$$n(z) = n_0\left(1 - \frac{z^2}{R^2}\right) \tag{176}$$

is called the Gerbier profile in the one dimensional Thomas Fermi approximation, where $R \approx \sqrt[3]{N}$ determines the boundaries of the condensate.

$$|\bar{\psi}_i|^2 = \frac{3}{4\bar{R}_{TF}}\left(1 - \left(\frac{\bar{z}}{\bar{R}_{TF}}\right)^2\right)\Bigg|_{i=1,2} \tag{177}$$

under the condition $|\bar{z}| < |\bar{R}_{TF}|$.

With the normalization $\int \bar{z}|\bar{\psi}_i|^2 = 1$ and

$$\frac{1}{2}\bar{z}^2 = \frac{2\omega_\perp}{\omega_{||}}\frac{a_s}{l_0}N\frac{3}{4\bar{R}_{TF}}\frac{\bar{z}^2}{\bar{R}_{TF}^2} \tag{178}$$

we obtain the Tomas-Fermi Radius of BEC that takes the following form

$$\bar{R}_{TF} = \sqrt[3]{3\frac{\omega_\perp}{\omega_{||}}\frac{a_s}{l_0}N} \tag{179}$$

This Radius determines the boundaries of the one–dimensional quasi–condensates and will be needed several times within the numerical calculation in the following chapter.

5 Computations

Numerical examples

For our numerical calculations we assume BECs of Rubidium ^{87}Rb atoms and therefore the following values in the cgs–system were used

scattering length : $a_s = 5.3 \times 10^{-7}\text{cm}$

trap frequencies : $\omega_\perp = 2\pi \times 2$ kHz , $\omega_{\shortparallel} = 2\pi \times 10$ Hz

mass : $m = 87 \times \text{m}_p = 87 \times 1.6726231 \times 10^{-24}\text{g}$

The Gaussian function was used as the starting point for our calculations at $\tau = 0$

$$\psi_i|_{i=1,2} = \frac{1}{\sqrt[4]{\pi}} e^{-\frac{1}{2}z^2} \tag{180}$$

All the calculations in this study where performed with the program Mathematica 9 by Wolfram Research.

5.1 Ground state

The first task in this study was to compute the ground states of our one–dimensional BECs, which were uncoupled at this point. Furthermore they were not influenced by the artificial gauge field, i.e. $J = 0$ and $\bar{k} = 0$. For both BECs the differential equation

$$i\hbar \frac{\partial}{\partial t}\psi_i = -\frac{\hbar^2}{2m}\nabla\psi_i + g|\psi_i|^2\psi_i + \frac{m\omega_{\shortparallel} z^2}{2}\psi_i, \qquad i = 1, 2 \tag{181}$$

had to be solved. The initial guess was the Gaussian profile in (180). The primary function of this step was to determine whether the used code (see appendix A.1) yields the correct result. This was verified by comparing the resulting distribution profile with the Gerbier profile (see (176) and (177)). This approximation is defined as follows

$$n\left(z\right) \propto \left(1 - \frac{z^2}{R^2}\right) \tag{182}$$

The result of this first step is depicted in Fig. 6 and the numerically computed ground–state profiles fit the Gerbier profile smoothly.

After the code structure was verified to deliver the correct result, the next task was to compute the density profiles of the ground states of the now coupled BECs with an active artificial gauge field applied to them.

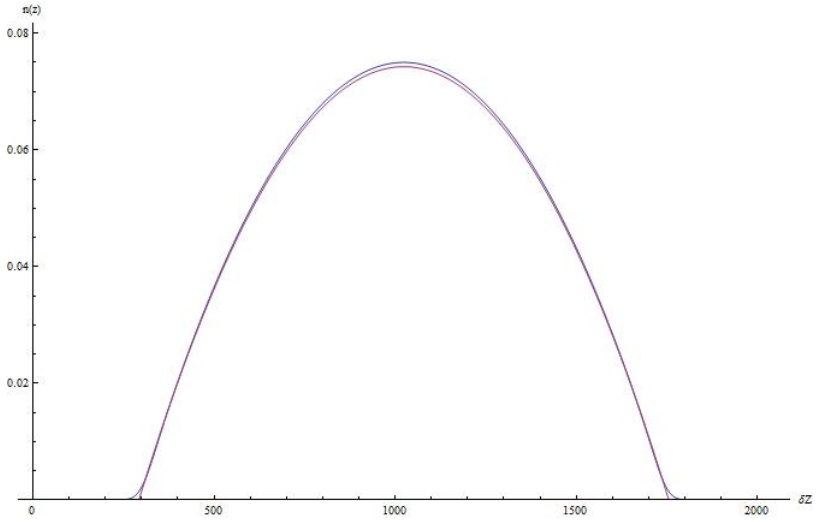

Figure 6: The blue line represents the density distribution of uncoupled and undisturbed ground states of our two 1D BECs. The purple line corresponds to the Gerbier profile.

5.2 Applying the artificial gauge field

For the code for the computation of the coupled BEC profiles see appendix A.2. First we had to establish the number of steps necessary in imaginary time to reach a stable result. By comparing the computed density profiles $n(z)|_{\tau_1}$ and $n(z)|_{\tau_2}$ for $\tau_1 < \tau_2$ the necessity of 150.000 steps was concluded. At this point of the imaginary time propagation the solutions of the coupled differential equations oscillated around stable solutions.

In our approach to numerically solve the coupled differential equations in (173) and (174) a time splitting spectral method of first order was used. In general that means the separable Hamiltonian of the investigated system is split up once. In our case the splitting was between the linear and non–linear parts of the Hamiltonian.

$$\hat{H} = \hat{H}_{lin} + \hat{H}_{nonlin} \tag{183}$$

So in both half steps the "distance" which the systems propagate in imaginary time are of equal value (See **3 Time Splitting Spectral Method**). For higher order of the splitting the step size must be adjusted. Constituting a simple example for a second order time splitting, we consider the following initial problem

$$\dot{f}(t) = (A + B + C) f(t) \tag{184}$$

$$f(t = 0) = f_0 \tag{185}$$

and for

- $\dot{v}(t) = Av(t) \quad \text{with} \quad v(t=0) = v_0$
  with the solution to this sub-problem $v(t) = e^{At}v_0$

- $\dot{w}(t) = Bw(t) \quad \text{with} \quad w(t=0) = w_0$
  with the solution to this sub-problem $w(t) = e^{Bt}w_0$

- $\dot{z}(t) = Cz(t) \quad \text{with} \quad z(t=0) = z_0$
  with the solution to this sub-problem $z(t) = e^{Ct}z_0$

The n^{th} cycle of the the imaginary time propagation leads to the function $f_n \approx f(t_n)$. Thereby we finally obtain the splitting of second order for the full problem to solve with the imaginary time step $\Delta\tau > 0$

$$f_n = e^{\frac{\Delta\tau}{2}A} e^{\frac{\Delta\tau}{2}B} e^{\Delta\tau C} e^{\frac{\Delta\tau}{2}B} e^{\frac{\Delta\tau}{2}A} f_{n-1} \tag{186}$$

To address the numerical accuracy of the herein used method, i refer to Bao et al. in [5], who state, while comparing several different numerical methods solving the Gross–Pitaevskii equation for defocusing BECs in 1D, that the numerical errors in the time splitting spectral method for the spatial and temporal discretization are of spectral order in space and second order in the imaginary time domain.

5.3 Results

For the particle number $N = 1100$ and the scaled strength of the artificial gauge field $\bar{k} = 5$, where $\bar{k}$ was introduced in (173) and (174), the numerically obtained ground state density profiles with increasing values of J are given in Fig. 7. In a real experiment the tunnelling coefficient between the two 1D BECs could be varied by changing the distance between the two condensates. If we set $N = 550$ while leaving the gauge field as before we obtain the density profile with respect to a changing tunnelling coefficient as can be seen in Fig. 8.

For completeness' sake the following two figures show the computational result for $\bar{k} = 10$ with $N = 1100$ in Fig. 9 and $N = 550$ in Fig. 10

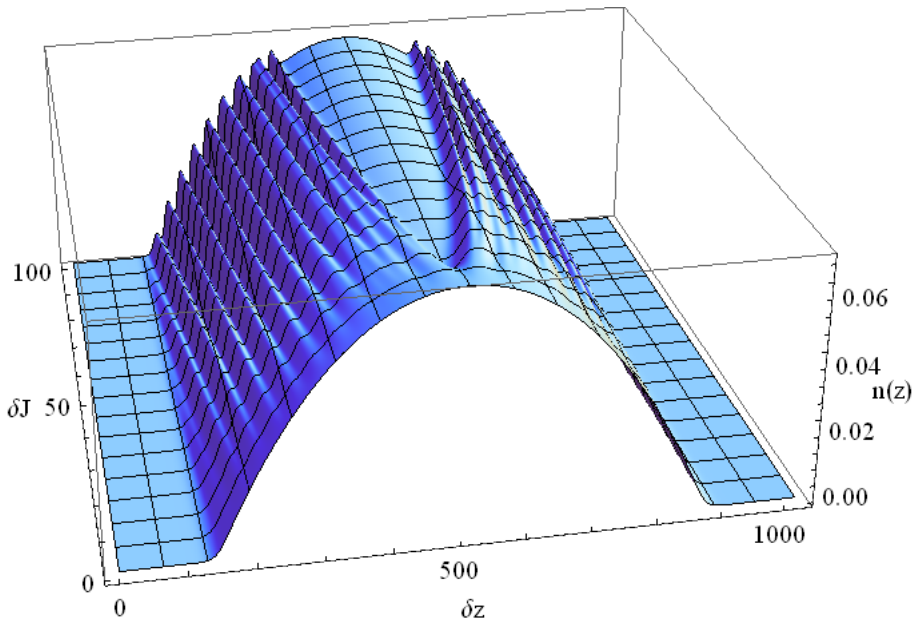

Figure 7: This plot shows the density profile under the increasing change of J, the tunnelling matrix coefficient. The particle number N was set to 1100 and the artificial gauge field strength $\bar{k}$ to 5. The step size in J is fixed with $\delta J = 0.1$ and therefore the range of J is [0,10], whereas the z–axis was split up into 2^{10} steps.

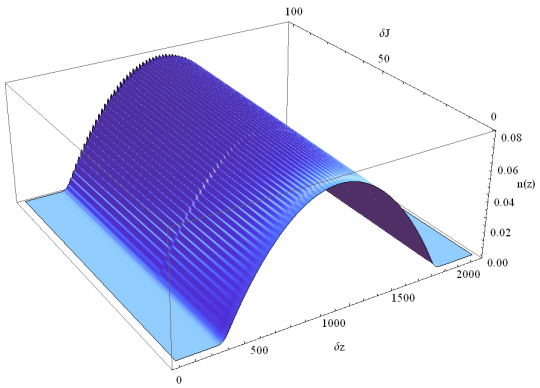

Figure 9: Plot for $N = 1100, \bar{k} = 10$, Range J: $[0, 10]$, number of steps in z equals 2^{11}

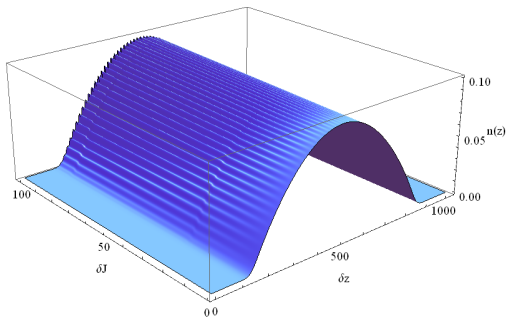

Figure 10: Plot for $N = 550$, $\bar{k} = 10$, Range J: $[0, 10]$, number of steps in z equals 2^{10}

5.4 Interpretation

The density profiles in the plots in Fig. 7, 8, 9 and 10 for zero coupling, i.e. $J = 0$, resemble the result which was obtained in the unperturbed ground state computation (see Fig. 6). With increased coupling the particle density distributions begin to show an oscillating character. This emerging spatial density modulation was discussed in one or another form by several authors (e.g. [27], [6]). Giovanazzi et al. point out the similarity of a quasi–one–dimensional density modulated BEC to a super solid in [14],

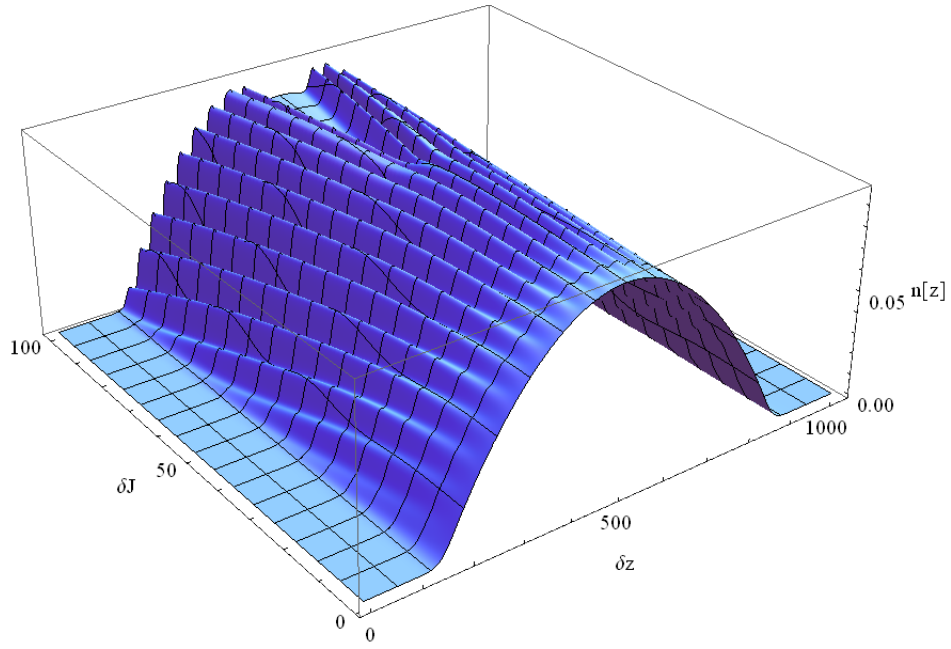

Figure 8: This plot shows the density profile for a particle number $N = 550$ and the artificial gauge field strength $\bar{k} = 5$. Step sizes δJ and δz are the same as in Fig. 8

which was described by Penrose and Onsager (see [25]). The lack of long–range configurational order in super fluids renders the existence of Bose–Einstein condensation in an ideal crystal impossible. They assumed that the super solid must consist of at least one particle at every lattice site at zero temperature. Later works showed that the consideration of lattice defects leads to opposite results, always assuming only one particle per lattice site. Kalinski et al. mention in [21] the temptation to call spatial modulated BECs super solids but the similarity lies in the spatial modulation and the phase coherence only. On the other hand the work of Góral et al. [15] shows that ultra cold atoms in an optical lattice can undergo several phases, not solely based on the s–wave scattering, but also due to long range dipole–dipole interactions [21]. These spatial modulations of the density are also present in the profiles computed numerically. This suits the initial idea, that the particles inside the BECs begin to migrate due to the applied artificial gauge field. The numerically computed results with gauge field strength $\bar{k} = 5$ (see Fig. 7 and 8) exhibit a macroscopic change in the particle distributions for different threshold values of J. These macroscopic transitions correspond to the anticipated quantum phase transitions we were looking for.

For an explanatory approach of this behaviour it is important to mention that the migration of particles in one of the BECs, the tunnelling into the other condensate and their movement in the second condensate in the opposite direction and finally the re–tunnelling into the initial condensate creates special two–dimensional vortex structure, so to say an array of vortices and anti–vortices, as can be seen in schematics in

Fig. 5. We can assume, that the vortices all carry the same charge $q = 1$, but with different signs, because, as has been shown, multiple quantized vortices, i.e. $q > 1$ are energetically unfavourable in harmonic trapping and therefore decay into single charged vortices.
In a short excursion let's discuss superconductivity. Both type I and type II superconductors are for $T < T_{CSC}$, where T_{CSC} is the critical temperature for superconductivity, in the Meissner–phase, in which an applied magnetic field below a certain critical value H_{c1} is expelled from the superconductor, which is mainly field free. This magnetic field decay is described by the London equation:

$$\nabla^2 H = \frac{1}{\lambda_L^2} H \tag{187}$$

The field penetrates the material only to a certain depth, called λ_L the London penetration length. For most superconducting materials λ_L is of the order of $100nm$. Above H_{c1} a type II superconductor changes into a mixed state, described by Abrikosov in 1957 in [1]. This state is also called vortex state, because in this regime, regions of the superconductor are normal and encircled by vortices of supercurrent. Qiang Du points out that quantized vortices in BECs, a key signature of superfluidity, are a macroscopic manifestation of quantum-mechanical behaviour, which is very well described by the Gross–Pitaevskii equation (see [13]). He emphasizes a certain similarity to the Ginzburg–Landau model, which is commonly used to describe high–temperature and low–temperature superconductors. The Abrikosov vortex model can be used as a reference for our results. Therefore the Abrikosov vortex, with its non-superconducting core can be seen as an analogy to the quantized vortices in super fluids, with a central node with zero density. Since the tunnelling region between the two 1D BECs is free of particles, therefore the density is zero, it can be assumed that the cores of the vortices are situated in this empty space.

In Fig. 7, 8 and 11 we can see the transition between two regimes. Especially Fig. 7 shows explicitly that the spatially modulated profile changes into a uniform profile. This raises the question, if the uniform regime is the energetically favourable or if the higher coupling between the two condensates, corresponding to an increasing value of J, prevents the emergence of quantized vortices.

To gain the threshold value for J, we compute the minimal energy of both cases for the following Hamiltonian

$$H = \sum_{j=1}^{2} \int dz \left[-\psi_j^\star \left(\partial z \pm i k_0 \right)^2 \psi_j + \frac{g}{2} |\psi_j|^4 \right] - \int dz \hbar J \left(\psi_1^\star \psi_2 + \psi_2^\star \psi_1 \right) \tag{188}$$

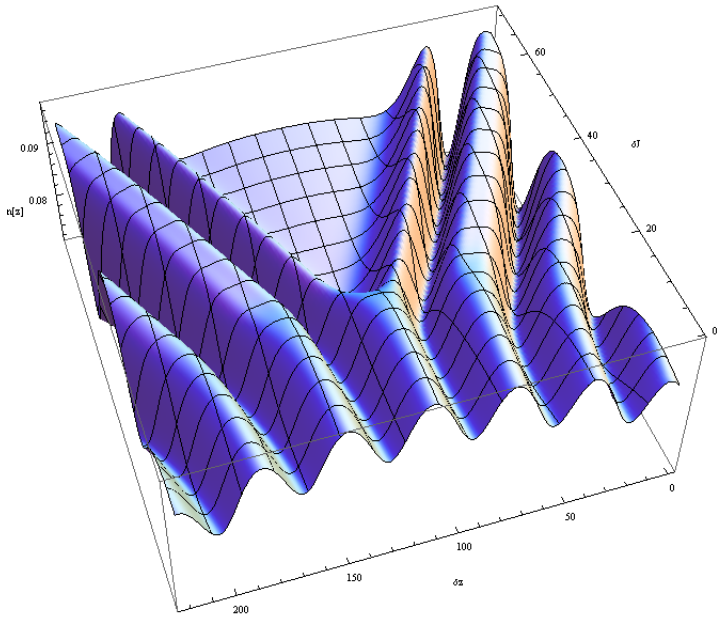

Figure 11: An enlarged view of the *split* in the spatial modulation of the density profile for the $N = 550$ and $\bar{k} = 5$ system. We see the onset of a transition from the spatial modulated density profile to a uniform one.

The ansatz for the spatial modulated wave functions is

$$\psi_j = \sqrt{\bar{n}}\sqrt{1 + \epsilon\cos\left(2k_0 z\right)}e^{\pm ik_0 z}, \tag{189}$$

and for the uniform profile the wave functions are

$$\psi_j = \sqrt{\bar{n}} \tag{190}$$

where $j = 1, 2$ and $\bar{n}$ is the uniform density.
In the first case the minimal energy is approximately given by

$$E_{min}^{mod} = -\frac{\frac{1}{2}\left(\hbar J\right)^2 \bar{n}}{\frac{\hbar^2 k_0^2}{m} + g\bar{n}}, \tag{191}$$

where in the latter case the minimal energy is given by

$$E_{min}^{uni} = \frac{\hbar^2 k_0^2}{m}\bar{n} - 2\hbar J\bar{n}. \tag{192}$$

Since we assume the phase transition to be caused by changing into the energetically favourable phase, we demand $E_{min}^{uni} \leq E_{min}^{mod}$ and obtain the formula for the threshold

value of the coupling coefficient J, where the two minimal energies are equal.

$$\hbar J_{cr} \simeq \frac{\hbar^2 k_0^2}{2m}\left(1+\frac{\frac{1}{4}\frac{\hbar^2 k_0^2}{m}}{\frac{\hbar^2 k_0^2}{m}+g\bar{n}}\right) \tag{193}$$

From the approximation above where the spatial modulated profile transforms into the energetically favourable uniform density profile, we see that the fraction of $\hbar J_{cr}/\left(\frac{\hbar^2 k_0^2}{2m}\right)$ tends to 1 for large densities $\bar{n}$. The scaled plots in Fig. 12 show that for $N = 1100$ particles in the two BECs with a uniform density of $\bar{n}_{1100} \simeq 0.050$ the fraction, which was mentioned before, should have the value of about $1,2120$, whereas in the halved particles number case for a uniform density of $\bar{n}_{550} \simeq 0.0625$ the fraction should be ~ 1.1839. From our numerically computed density profiles the fraction

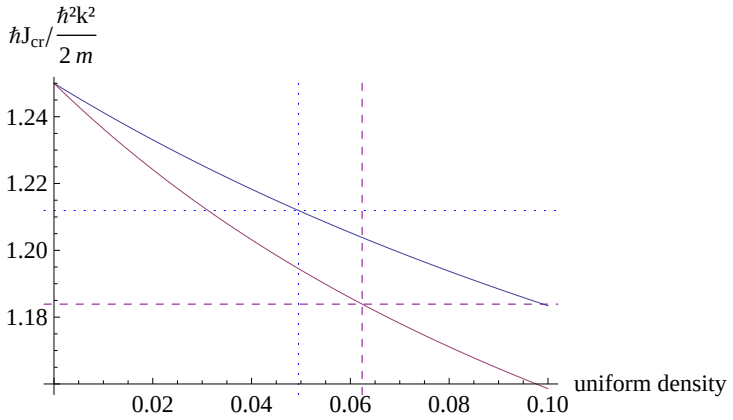

Figure 12: These two lines correspond to the theoretical threshold values of J_{cr} in units of $\hbar\bar{J}_{cr}/\left(\frac{\hbar^2\bar{k}_0^2}{2m}\right)$ plotted against the density $\bar{n}$(c.f. (193)). Through the particle number dependence of $\bar{k}$ we see two lines. The $N = 1100$ case and the $N = 550$ case are depicted by the blue line and the purple line respectively. The crossing points of the dotted and dashed line show the theoretically computed values of the colour matching cases.

$$\left.\frac{\hbar\bar{J}_{cr}}{\frac{\hbar^2\bar{k}^2}{2m}}\right|_{N=500} \simeq 1.9304, \tag{194}$$

where the particle–number–dependent $\bar{k}$ is defined via $\bar{k} = 1.4kR_{TF}/\pi$. The factor between the numerical value of the fraction f_{num} in (194) and the value f_{th} is approximately given by $f_{num} \simeq 1.630 f_{th}$. This discrepancy can be based on the numerical errors from the time split spectral method. Just for sake of completeness, it should be mentioned, that the difference between the theoretical and numerical value in the $N = 1100$ case is too extensive to be addressed.

6 Outlook

The prudent next step to take is to repeat the computations with a split method of higher order to receive threshold values of $\bar{J}_{cr}$, which are more compatible with the theoretical description. Another topic of interest for future studies following this is the computation of the excitation spectrum of the system investigated in this thesis.
Moreover the experimental verification of the results gained from the numerical computations in this work would be of interest. Based on the technique of the Atomchip (see [29]), which is used in several experiments concerning ultra-cold atoms and BEC, by the group around Jörg Schmiedmayer at the Institute of Atomic and Subatomic Physics of the Technical University Vienna would be a suitable starting point for the experimental realization.
Especially Berrada et al. in [7] have used the Atomchip to build a Mach–Zehnder interferometer for BECs by tuning the potential, created by the Atomchip, with a radio frequency–field into a double well potential. Therefore the BEC in the previous single well is coherently split and afterwards spatially separated. As required in a Mach–Zehnder interferometer a phase–shift is applied to one of the newly created BECs and they are then recombined. The controllability of the spatial distance of the two wells and also the height of the potential peak between them in the setup of Berrada et al. can be used to tune the J–parameter and measure the quantum phase transition numerically found in the calculation in this thesis.

A Mathematica code

A.1 Ground state

```
Nhalf = 2^10;
Nfull = 2Nhalf;
RTF = 10.;
L = 2.8RTF;
Kmin = .5(2Pi/L)^2;
dz = L/Nfull;
Umin = .5dz^2;
NLC = (2/3)RTF^3;

dt = .3/RTF^3;
Tdt = 15000;

psi0 = Table[Exp[-.5(dz(j - Nhalf))^2]/(Pi^(1/4)), {j, Nfull}];

Do[
Do[
psi0[[j]] = psi0[[j]]Exp[-dt(Umin(j - Nhalf)^2 + NLC * Abs[psi0[[j]]]^2)],
{j, Nfull}];
psi1 = Fourier[psi0];
Do[psi1[[j]] = psi1[[j]]Exp[-dtKmin(j - 1)^2], {j, Nhalf}];
Do[psi1[[j]] = psi1[[j]]Exp[-dtKmin(Nfull + 1 - j)^2],
{j, Nhalf + 1, Nfull}];
psi0 = InverseFourier[psi1];
I0 = Sqrt[dzSum[Abs[psi0[[j]]]^2, {j, Nfull}]];
psi0 = psi0/I0; , {i, Tdt}]
```

A.2 Coupled BECs

```
num = 2^10;
NUM = 2num;
ωWert = 2π10;
ωpWert = 2π2000;
NWert = 1100;
LWert = Sqrt[HWert/(mWert ωWert)];
Randrep = LWert (15NWertasl/LWert)^(1/5);
Rtf = (3ωpWert/ωWert asl/LWert NWert)^(1/3);
RtfLWert
τWert = 0.3/Rtf^3;

κ = KWert/δK
Ct = Cosh[JWertτWert]
St = Sinh[JWertτWert]

δZ = (2.8Rtf)/NUM//N;
δK = ((2Pi)/(δZNUM))//N;
KNO = Table[(j - num/2) δZ, {j, 1, num}];
ZN = Table[(j - num/2) δZ, {j, 1, num}];
TΔτ = 150000;

ψR0 = Table[Exp[-1/2 (δZ(j-num))^2]/π^(1/4), {j, NUM}];
ψL0 = Table[Exp[-1/2 (δZ(j-num))^2]/π^(1/4), {j, NUM}];
Do[
Do[
ψR0[[j]] = ψR0[[j]]Exp[-τWert (2/3 Rtf^3Abs[ψR0[[j]]]^2 + 1/2 (δZ(j - num))^2)];
ψL0[[j]] = ψL0[[j]]Exp[-τWert (2/3 Rtf^3Abs[ψL0[[j]]]^2 + 1/2 (δZ(j - num))^2)];
, {j, NUM}];
```

```
Do[
ψR0[[j]] = CtψR0[[j]] + StψL0[[j]];
ψL0[[j]] = CtψL0[[j]] + StψR0[[j]],
{j, NUM}];

ψR1 = Fourier[ψR0];
ψL1 = Fourier[ψL0];

Do [ψR1[[j]] = Exp [-τWert½δK^2 (j - 1 - κ)^2] ψR1[[j]], {j, num}] ;
Do [ψR1[[j]] = Exp [-τWert½δK^2(j - NUM - 1 - κ)^2] ψR1[[j]], {j, num + 1, NUM}] ;

Do [ψL1[[j]] = Exp [-τWert½δK^2 (j - 1 + κ)^2] ψL1[[j]], {j, num}] ;
Do [ψL1[[j]] = Exp [-τWert½δK^2(j - NUM - 1 + κ)^2] ψL1[[j]], {j, num + 1, NUM}] ;

ψR0 = InverseFourier[ψR1];
ψL0 = InverseFourier[ψL1];

NR0 = Sqrt[Total[δZAbs[ψR0]^2]];
NL0 = Sqrt[Total[δZAbs[ψL0]^2]];

ψR0 = ψR0/NR0;
ψL0 = ψL0/NL0; ,{i, TΔτ}]
```

References

[1] Abrikosov, A. A., The magnetic properties of superconducting alloys, J. Phys. Chem. Solids, 2, 199-208, 1957

[2] Aspect, A. and Arimondo, E. and Kaiser, R. and Vansteenkiste, N. and Cohen-Tannoudji, C., Laser Cooling below the One-Photon Recoil Energy by Velocity-Selective Coherent Population Trapping, Phys. Rev. Lett., 61, 7, 826–829, American Physical Society,1988.

[3] Bader,P. and Blanes, S. and Casas, F., Solving the Schrödinger eigenvalue problem by the imaginary time propagation technique using splitting methods with complex coefficients, J. Chem. Phys., 139, 124117, 2013.

[4] Bao, W. and Du, Q.,Computing the Ground State Solution of Bose–Einstein Condensates by a Normalized Gradient Flow,SIAM Journal on Scientific Computing, 25,5, 1674-1697,2004.

[5] Bao, W. and Jaksch, D. and Markowich, P. A., Numerical Solution of the Gross-Pitaevskii Equation for Bose-Einstein Condensation, J. Comput. Phys., 187, 1, 318 - 342, 2003.

[6] Barrett, M. D. and Sauer, J. A. and Chapman, M. S., All-Optical Formation of an Atomic Bose-Einstein Condensate, Phys. Rev. Lett., 87, 1, 010404, 2001

[7] Berrada, T. and van Frank, S. and Bücker, R. and Schumm, T. and Schaff, J.–F. and Schmiedmayer, J., Integrated Mach–Zehnder interferometer for Bose–Einstein condensated, Nature Communications 4, 2077, 2013

[8] Bose, S. N., Plancks Law and Light Quantum Hypothesis, Z. Phys., 26:178, 1924

[9] Dalfovo, F. and Giorgini, S. and Pitaevskii, L. P. and Stringari, Theory of Bose-Einstein condensation in trapped gases, S.,Rev. Mod. Phys.,71,3,463–512,American Physical Society,1999.

[10] Dalfovo, F. and Stringari, S.,Bosons in anisotropic traps: Ground state and vortices, Physical Review A (Atomic, Molecular, and Optical Physics),53,4, 2477-2485, 1996.

[11] Dalibard, J. and Cohen-Tannoudji, C., Dressed-atom approach to atomic motion in laser light: the dipole force revisited, J. Opt. Soc Am. B., 2, 11, 1707–1720, 1985.

[12] Dalibard, J. and Gerbier, F. and Juzeliūnas, G. and Öhberg, P.,Colloquium: Artificial gauge potentials for neutral atoms, Rev. Mod. Phys., 83,4,1523–1543, American Physical Society,2011.

[13] Du. Q., Quantized vortices in BEC and superconductors, Proc. Appl. Math. Mech. 7 ,1023901-1023902, 2007

[14] Giovanazzi, S. and O'Dell, D. and Kurizki, G., Density Modulations of Bose-Einstein Condensates via Laser-Induced Interactions, Phys. Rev. Lett., 88, 13, 130402, 2002

[15] Góral, K. and Santos, L. and Lewenstein, M., Quantum Phases of Dipolar Bosons in Optical Lattices, Phys. Rev. Lett., 88, 17, 170406, 2002

[16] Greiner, M. and Mandel, O. and Esslinger, T. and Hänsch, T. W. and Bloch, I., Quantum phase transitions from a superfluid to a Mott insulator in a gas of ultracold atoms, Nature, 415, 39-44, 2002

[17] Jackson, B. and McCann, J. F. and Adams, C. S., Dissipation and vortex creation in Bose–Einstein condensed gases. Physical Review A 61: 051603,2000.

[18] Jordan P. and Wigner E., Z. Phys.47, 631, 1928

[19] Ketterle, W. and van Druten, N.J., Bose-Einstein condensation of a finite number of particles trapped in one or three dimensions, Phys. Rev. A 54, 656-660, 1996.

[20] Kalinski, M. and Mazets, I.E. and Kurizki, G. and Malomed, B.A. and Vogel, K. and Schleich, W.P., Dynamics of laser–induced lattice formtion in Bose–Einstein condensates, arXiv:cond-mat/0310480v2, 2004

[21] Kurizki, G. and Mazets, I.E. and O'Dell, D.H.J. and Schleich, W.P., Bose–Einstein condensates with laser–induced dipole–dipole interactions beyond the mean–field approach, Int. J. Mod. Phys. B, 18, 961, 2004.

[22] Mazets, I.E. and O'Dell, D.H.J. and Kurizki, G. and Davidon, N. and Schleich, W.P., Depletion of a Bose-Einstein condensate by laser-induced dipole-dipole interactions, J. Phys. B: At. Mol. Opt. Phys. 37, 155, 2004

[23] Parker, N. G. and Jackson, B. and Martin, A. M. and Adams, C. S., Vortices in Bose–Einstein Condensates: Theory, arXiv:0704.0146, 2007.

[24] Pethick, C. J. and Smith, H., Bose-Einstein Condensation in Dilute Gases, Cambridge University Press, 2002

[25] Penrose, O. and Onsager, L., Bose-Einstein Condensation and Liquid Helium, Phys. Rev., 104, 3, 576–584, 1956

[26] Pitaevskii, L. and Stringari, S., Bose-Einstein Condensation, Clarendon Press, Oxford, 2003.

[27] Stenger, J. and Inouye, S. and Stamper-Kurn, D. M. and Miesner, H.-J. and Chikkatur, A. P. and Ketterle, W., Spin domains in ground-state Bose-Einstein condensates, Nature, 396, 345-348, 1998

[28] Stimming, H.–P. and Mauser, N. J. and Schmiedmayer, J. and Mazets, I. E., Dephasing in coherently split quasicondensates, Phys. Rev. A, 83, 023618. 2011

[29] Tinker, M. and Groth, S. and Haslinger, S. and Manz, S. and Betz, T. and Schneider, S. and Bar–Joeph, I. and Schumm, T. and Schiedmayer, J., Multilayer atom chips for versatile micromanipulation, Appl. Phys. Lett. 92, 254102, 2008

[30] Yamamoto, Y., Lecturenotes: Bose-Einstein Condensation and Lasers, Stanford University, Winter 2010

List of Figures

1 Multi level system – Dalibard, J. and Gerbier, F. and Juzeliūnas, G. and Öhberg, P.,Colloquium: Artificial gauge potentials for neutral atoms, Rev. Mod. Phys., 83,4,1523–1543, American Physical Society,2011, p. 1529. 13

2 Zeemann–slower – Pethick, C. J. and Smith, H., Bose-Einstein Condensation in Dilute Gases, Cambridge University Press, 2002, p. 59. 21

3 MOT – Pethick, C. J. and Smith, H., Bose-Einstein Condensation in Dilute Gases, Cambridge University Press, 2002, p. 79. 25

4 Evaporative cooling – Pethick, C. J. and Smith, H., Bose-Einstein Condensation in Dilute Gases, Cambridge University Press, 2002, p. 91. . . 27

5 Schematic drawing of the tunnel coupled 1D BECs 34

6 Dual plot undisturbed and uncoupled groundstate density profile and Gerbier profile 40

7 3D plot: density profile, N=1100, $\bar{k} = 5$ 42

9 3D plot: density profile, N=1100,$\bar{k} = 10$ 42

10 3D plot: density profile, N=550, $\bar{k} = 10$ 42

8 3D plot: density profile, N=550, $\bar{k} = 5$ 43

11 3D plot: The split region of density profile, N=550, $\bar{k} = 5$ 45

12 Plot of fractions of $\hbar\bar{J}$ and $\left(\hbar^2\bar{k_i}^2\right)/(2m)$ for the theoretical threshold values of J plotted against the uniform density of 1D BECs 46

Curriculum Vitae

Personal

Name:	Beck Stefan BSc.
Date of Birth:	September 28^{th}, 1979
Nationality:	Austria

Education

9/1985 - 6/1990	Primary School (VS St. Ulrich bei Steyr, Oberösterreich)
9/1990 - 6/1993	High School (BG Werndlpark Steyr, Oberösterreich)
9/1993 - 6/1994	Middle School (HS Ennsleite Steyr, Oberösterreich)
9/1994 - 6/1999	High School (BRG Michaelerplatz Steyr, Oberösterreich)
6/2005	A-Levels (Matura)
10/1999 - 4/2013	Diploma Studies in Physics at the University of Vienna
5/2013 - 7/2013	Bachelor Studies in Physics at the University of Vienna
7/2013	Award of the academic degree BSc in Physics
Since 10/2013	Master Studies in Physics at the University of Vienna